Arteriosclerosis, Thrombosis, and Vascular Biology

BASIC SCIENCES

Rap1A Modulates Store-Operated Calcium Entry in the Lung Endothelium: A Novel Mechanism Controlling NFAT-Mediated Vascular Inflammation and Permeability

Ramoji Kosuru, Olivier Romito, Guru Prasad Sharma, Francesca Ferraresso, Behshid Ghadrdoost Nakhchi, Kai Yang, Tadanori Mammoto, Akiko Mammoto, Christian J. Kastrup, David X. Zhang, Paul H. Goldspink, Mohamed Trebak, Magdalena Chrzanowska

BACKGROUND: Store-operated calcium entry mediated by STIM (stromal interaction molecule)-1–Orai1 (calcium release-activated calcium modulator 1) is essential in endothelial cell (EC) functions, affecting signaling, NFAT (nuclear factor for activated T cells)-induced transcription, and metabolic programs. While the small GTPase Rap1 (Ras-proximate-1) isoforms, including the predominant Rap1B, are known for their role in cadherin-mediated adhesion, EC deletion of Rap1A after birth uniquely disrupts lung endothelial barrier function. Here, we elucidate the specific mechanisms by which Rap1A modulates lung vascular integrity and inflammation.

METHODS: The role of EC Rap1A in lung inflammation and permeability was examined using in vitro and in vivo approaches.

RESULTS: We explored Ca^{2+} signaling in human ECs following siRNA-mediated knockdown of Rap1A or Rap1B. Rap1A knockdown, unlike Rap1B, significantly increased store-operated calcium entry in response to a GPCR (G-protein–coupled receptor) agonist, ATP (500 µmol/L), or thapsigargin (250 nmol/L). This enhancement was attenuated by Orai1 channel blockers 10 µmol/L BTP2 (N-[4-[3,5-bis(trifluoromethyl)-1H-pyrazol-1-yl]phenyl]-4-methyl-1,2,3-thiadiazole-5-carboxamide), 10 µmol/L GSK-7975A, and 5 µmol/L Gd^{3+}. Whole-cell patch clamp measurements revealed enhanced Ca^{2+} release-activated Ca^{2+} current density in siRap1A ECs. Rap1A depletion in ECs led to increased NFAT1 nuclear translocation and activity and elevated levels of proinflammatory cytokines (CXCL1 [C-X-C motif chemokine ligand 1], CXCL11 [C-X-C motif chemokine 11], CCL5 [chemokine (C-C motif) ligand 5], and IL-6 [interleukin-6]). Notably, reducing Orai1 expression in siRap1A ECs normalized store-operated calcium entry, NFAT activity, and endothelial hyperpermeability in vitro. EC-specific Rap1A knockout ($Rap1A^{i\Delta EC}$) mice displayed an inflammatory lung phenotype with increased lung permeability and inflammation markers, along with higher Orai1 expression. Delivery of siRNA against Orai1 to lung endothelium using lipid nanoparticles effectively normalized Orai1 levels in lung ECs, consequently reducing hyperpermeability and inflammation in $Rap1A^{i\Delta EC}$ mice.

CONCLUSIONS: Our findings uncover a novel role of Rap1A in regulating Orai1-mediated Ca^{2+} entry and expression, crucial for NFAT-mediated transcription and endothelial inflammation. This study distinguishes the unique function of Rap1A from that of the predominant Rap1B isoform and highlights the importance of normalizing Orai1 expression in maintaining lung vascular integrity and modulating endothelial functions.

GRAPHIC ABSTRACT: A graphic abstract is available for this article.

Key Words: calcium ■ capillary permeability ■ endothelial cells ■ lipid nanoparticles ■ mice ■ monomeric GTP-binding proteins ■ pneumonia

Correspondence to: Magdalena Chrzanowska, PhD, Versiti Blood Research Institute, PO Box 2178, Milwaukee, WI 53201. Email mchrzanowska@versiti.org
Supplemental Material is available at https://www.ahajournals.org/doi/suppl/10.1161/ATVBAHA.124.321458.
For Sources of Funding and Disclosures, see page 2285.

Arterioscler Thromb Vasc Biol is available at www.ahajournals.org/journal/atvb

Nonstandard Abbreviations and Acronyms

BALF	bronchoalveolar lavage fluid
CCL2	chemokine (C-C motif) ligand 2
CCL5	chemokine (C-C motif) ligand 5
CRAC	Ca^{2+} release-activated Ca^{2+}
EC	endothelial cell
ECIS	electrical cell impedance sensing
eNOS	endothelial NO synthase
ER	endoplasmic reticulum
GPCR	G-protein–coupled receptor
hCAEC	human coronary artery endothelial cell
hMVEC	human lung microvascular endothelial cell
IL-6	interleukin-6
LNP	lipid nanoparticle
NFAT	nuclear factor for activated T cells
PLCβ	phospholipase Cβ
RTK	receptor tyrosine kinase
SERCA	sarcoplasmic/ER Ca^{2+}-ATPase
SOCE	store-operated calcium entry
STIM	stromal interaction molecule
VEGF	vascular endothelial growth factor

Highlights

- Rap1A (Ras-proximate-1) deficiency in ECs leads to elevated store-operated calcium entry through upregulation of Orai1 (calcium release-activated calcium modulator 1) channel expression.
- Consequently, with elevated store-operated calcium entry, NFAT activity is elevated, contributing to increased inflammatory cytokine expression in Rap1A-deficient pulmonary ECs.
- Normalizing Orai1 expression in siRap1A ECs rescues elevated store-operated calcium entry and EC permeability.
- Elevated basal lung permeability and inflammation in $Rap1A^{i\Delta EC}$ mice are normalized by lipid nanoparticle delivery of siOrai1 to lung ECs in $Rap1A^{i\Delta EC}$ mice, suggesting Orai1 as potential therapeutic target for pulmonary conditions associated with EC dysfunction.

Lung inflammatory diseases such as pneumonia and chronic obstructive pulmonary disease are responsible for >3.2 million deaths every year, the third leading cause of death worldwide.[1] Underlying the lung inflammatory diseases is the endothelial proinflammatory phenotype, promoting the development of acute endothelialitis in the pulmonary microcirculation complicated by abnormal vasoconstrictor responses, luminal plugging by inflammatory cells, and intravascular thrombosis.[2–4] Therefore, effective intervention targeting lung endothelial cells (ECs) would be of fundamental significance for the treatment of respiratory diseases. Currently, no such approaches targeting lung ECs exist to combat lung inflammation.

See accompanying editorial on page 2288

Endothelial Ca^{2+} homeostasis is essential for angiogenesis, permeability, and NO release and primarily involves store-operated Ca^{2+} entry (SOCE) via highly Ca^{2+}-selective Ca^{2+} release-activated Ca^{2+} (CRAC) channels, the most ubiquitous Ca^{2+} entry pathway in nonexcitable cells like ECs.[5–13] Agonist-induced endothelial stimulation activates GPCRs (G-protein–coupled receptors) or RTKs (receptor tyrosine kinases), triggering inositol 1,4,5-triphosphate–induced Ca^{2+} release from intracellular stores and subsequent endoplasmic reticulum (ER) Ca^{2+} depletion.[14] This causes the Ca^{2+}-sensing ER-resident STIM (stromal interaction molecules) to translocate to ER-plasma membrane junctions, thus trapping and activating plasma membrane CRAC channels encoded by Orai (calcium release-activated calcium modulator 1) channels.[15–21]

SOCE not only replenishes depleted ER Ca^{2+} but also initiates signaling and transcriptional activities influencing physiological functions.[20–22] However, prolonged CRAC activity can cause Ca^{2+} overload and apoptosis.[23] Both loss- and gain-of-function mutations in either Orai1 or STIM1 lead to altered Ca^{2+} influx and subsequent activation of NFAT (nuclear factor for activated T cells), resulting in a spectrum of immune and muscular diseases.[24,25] Moreover, dysregulated SOCE has been implicated in endothelial inflammation through the upregulation of NFAT-mediated transcription and proinflammatory cytokine production.[22,26–32] Additionally, the nonselective cation channels of the transient receptor potential canonical family are also involved in Ca^{2+} entry in ECs.[33–38] Despite being originally involved in SOCE in earlier studies,[39,40] transient receptor potential canonical channels have been shown to operate independently of store depletion.[41,42] While the importance of SOCE in maintaining EC homeostasis is well recognized,[12] and several potential CRAC channel modifiers have been identified,[18] the specific mechanisms by which SOCE is regulated in ECs remain to be fully elucidated.

Rap1A (Ras-proximate-1) and Rap1B, 2 highly homologous Rap1 isoforms, are key to vascular homeostasis.[43] Initially recognized for cellular adhesion modulation,[44] Rap1 promotes VE-cadherin adhesion in ECs in vitro.[45,46] Constitutive endothelial deletion of both isoforms disrupts the vascular barrier and normal cardiovascular development.[47] Although Rap1 activation promotes barrier function during inflammation,[48] postnatal EC-Rap1 deletion does not markedly affect vascular barriers in most vascular beds, suggesting its nonessential role in maintaining cadherin-based junctions.[46] However, lung vascular permeability specifically occurs in EC-Rap1A KO mice, but not in EC-Rap1B knockouts,[46] hinting that Rap1A's unique functions in the lung are possibly

mediated through the C-terminal region of Rap1 that is slightly different in Rap1B.[45,49]

While not essential for maintaining cell-cell adhesion, Rap1 is crucial for eNOS (endothelial NO synthase)-derived NO production with distinct phenotypes in EC-specific Rap1A and Rap1B knockout mice.[50–52] Notably, Rap1A uniquely supports Ca^{2+}-dependent eNOS regulation,[52] leading to the hypothesis that disrupted Ca^{2+} signaling in Rap1A-deficient ECs may underlie lung vascular barrier defects in EC-Rap1A KO ($Rap1A^{i\Delta EC}$) mice.

Herein, taking advantage of $Rap1A^{i\Delta EC}$ mice and RNA silencing, we probed the distinct roles of Rap1 isoforms in Ca^{2+} signaling and endothelial inflammation. Our findings reveal divergent functions of Rap1A and Rap1B in agonist-induced SOCE. Rap1A notably limits Orai1 channel expression and activity, thus acting as a rheostat by dampening endothelial Ca^{2+} signaling and preventing excessive NFAT activation and subsequent inflammation. Our study uncovers a novel function of Rap1A in endothelial Ca^{2+} signaling and a novel mechanism of lung endothelial barrier regulation.

MATERIALS AND METHODS

Data Availability

The data that support the findings of this study are available from the corresponding author upon reasonable request.

Cell Culture and Transfection

Human lung microvascular ECs (hMVECs) and human coronary artery ECs (hCAECs) were obtained from Lonza (Walkersville, MD). We have previously shown that human umbilical vein ECs, human pulmonary artery ECs, and human dermal microvascular ECs all signal through STIM1 and Orai1 in the same manner.[12,53,54] Here, we used hCAECs for calcium measurements, as they show more reliable Ca^{2+} signals. We used hMVECs for NFAT nuclear translocation assay, NFAT luciferase assay, cytokine array, and electrical cell impedance sensing (ECIS) assay due to their physiological relevance for lung permeability and inflammation studies. hMVECs and hCAECs were cultured in full growth medium (EGM-2 MV [endothelial growth medium-2 microvascular]; Lonza) at 37 °C in a humidified incubator with 5% CO_2. All cells between passages 4 and 8 were used for all in vitro experiments. Forty percent to 50% confluent EC monolayers were transfected with 50 nmol/L Rap1A, 50 nmol/L Rap1B siGENOME siRNA pool, or with nontargeting siRNA pool (Dharmacon) complexed with lipofectamine 2000 (0.5 g/mL; Invitrogen) for 6 hours in 1× OPTIMEM and cultured for an additional 30 hours in complete EGM-2 MV culture medium at 37 °C. After 24 hours of siRap1A knockdown, the ECs were further transfected with 2 nmol/L Orai1 siRNA (Dharmacon) and cultured for an additional 12 hours before performing functional analysis.

Ca^{2+} Measurements

Ca^{2+} measurements in ECs were performed using a previously published protocol.[55,56] siControl and siRap1A hCAECs were seeded onto round 35-mm glass bottom petri dishes (FluoroDish) 24 hours before imaging at a concentration of 50×10^3 cells. The cells were incubated and loaded with the ratiometric Ca^{2+} indicator Fura-2 AM (Fura-2-acetoxymethyl ester; 2 µmol/L; Molecular Probes) in a HEPES-buffered saline solution containing 120 mmol/L NaCl, 5.4 mmol/L KCl, 0.8 mmol/L $MgCl_2$, 1 mmol/L $CaCl_2$, 20 mmol/L HEPES, and 10 mmol/L D-glucose, at pH 7.4 for 30 minutes at room temperature. Following Fura-2 loading, cells were washed 3× with HEPES-buffered saline solution and mounted on a fluorescence microscope (Nikon TE200). Fura-2 fluorescence was measured every 2 s by excitation at 340 and 380 nm using a fast shutter wheel (LambdaDG-4; Sutter Instruments), and the emission at 510 nm was collected through a 20× fluorescence objective. Fluorescence data were collected from individual cells on a pixel-by-pixel basis and processed using the Metafluor software (Universal Imaging). At least 450 cells from 3 independent experiments were analyzed. All cytosolic Ca^{2+} concentrations are presented as the ratio of F_{340}/F_{380}.

We used Ca^{2+} add-back protocol to record Ca^{2+} release from the ER and Ca^{2+} entry from the extracellular medium separately. First, we stimulated the ECs with ATP (500 µmol/L) or thapsigargin (250 nmol/L) in the presence of zero Ca^{2+} HEPES-buffered saline solution buffer to record Ca^{2+} release from the ER. When the F_{340}/F_{380} ratio reached the basal level, we introduced 2 mmol/L Ca^{2+} HEPES-buffered saline solution buffer containing ATP or thapsigargin to record Ca^{2+} entry. hCAECs were stimulated with ATP for 10 to 12 minutes or thapsigargin for 8 to 10 minutes, as indicated in individual fluorescence plots. Ca^{2+} channel blockers, BTP2 (N-[4-[3,5-bis(trifluoromethyl)-1H-pyrazol-1-yl]phenyl]-4-methyl-1,2,3-thiadiazole-5-carboxamide; 10 µmol/L), GSK-7975A (10 µmol/L), and Gd^{3+} (5 µmol/L) were added at the peak height of Ca^{2+} entry for 2 minutes. ATP and Gd^{3+} were diluted in water, whereas thapsigargin and GSK-7975A were diluted in 10% dimethyl sulfoxide.

Patch Clamp Electrophysiology

Whole-cell patch clamp recordings were performed with Axopatch 200B and Digidata 1440A (Molecular Devices) as described previously.[12] Experiments were monitored with pCLAMP10, and the analysis was performed using the Clampfit 10.1 software (https://www.moleculardevices.com). Patch pipettes (2–5 MΩ) were pulled from borosilicate glass capillaries (World Precision Instruments) with a P-1000 Flaming/Brown micropipette puller (Sutter Instruments) and were filled with pipette solution of the following composition: 150 mmol/L Cs-methanesulfonate, 20 mmol/L BAPTA (1,2-bis(o-aminophenoxy)ethane-N,N,N′,N′-tetraacetic acid) a, 8 mmol/L $MgCl_2$, and 10 mmol/L HEPES (pH adjusted to 7.2 with CsOH). Before recordings, hCAEC transfected cells were trypsinized and seeded in bottom glass coverslips for 30 minutes, allowing cell adhesion. To improve the seal stability, 3 µmol/L nimodipine was added in the bath solution containing 105 mmol/L Na-methanesulfonate, 10 mmol/L CsCl, 1.2 mmol/L $MgSO_4$, 20 mmol/L Ca^{2+}, 10 mmol/L D-glucose, and 10 mmol/L HEPES (pH adjusted to 7.4 using NaOH). We selected exclusively cells with a tight seal (>3 GΩ) and small series resistance (<8 MΩ) to perform the recordings. The cells were maintained at a holding potential of 0 mV before stimulation with a voltage ramp from −150 to +50 mV (lasting 800 ms, applied every 3 s). To amplify Ca^{2+} current during experiments, the bath solution was switched to a divalent-free

solution containing 135 mmol/L Na-methanesulfonate, 10 mmol/L HEDTA (N-(2-hydroxyethyl)ethylenediaminetriacetic acid), 1 mmol/L EDTA, and 10 mmol/L HEPES (pH adjusted at 7.4 with HCl).

Reverse Transcription Quantitative Polymerase Chain Reaction

Total RNA was extracted from siControl and siRap1A ECs using RNeasy Mini Kit (Qiagen) according to the manufacturer's instructions. The quantity and quality of extracted RNA were evaluated using NanoDrop spectrophotometer (Thermo Fisher Scientific). Then, cDNA was prepared from purified RNA using Omniscript RT Kit (Qiagen) according to the manufacturer's instructions. Reaction products were stored at −20 °C until the analysis. Primers were acquired from Integrated DNA Technologies (Table S1). QuantStudio 6 Flex and SYBR GREEN (both from Applied Biosystems) were used to conduct the real-time qPCR (quantitative polymerase chain reaction). Samples were analyzed using the following protocol: initial denaturation at 95 °C for 20 s, 40 cycles of amplification including denaturation at 95 °C for 1 s, then primer annealing at 60 °C for 20 s, and extension steps at 95 °C for 15 s. Transcript fold change was calculated relative to the siControl and normalized to β-actin using the $^{\Delta\Delta}$Ct method.[57]

Western Blotting

Orai1 protein expression in ECs and lung tissues was assessed by Western blotting. Tris-glycine 4% to 12% gradient gels were used to resolve cell lysates and blotted onto nitrocellulose membranes as described previously.[58] The following antibodies were used for Western blot analysis: antibodies against Orai1 (1:1000; Sigma-Aldrich; No. O8264), Rap1A/Rap1B (1:1000; Cell Signaling Technologies; No. 2399), and β-actin (1:1000; Santa Cruz Biotechnology; No. sc-47778). Horseradish peroxidase-conjugated secondary antibodies (1:10 000) followed by chemiluminescence detection using the Amersham Imager 600 analysis software (GE Healthcare) were used for densitometry. Blanked values (following subtraction of the corresponding empty well lane value) were normalized within each experiment and used to calculate fold change in protein expression between Rap1A-deficient and control conditions.

Surface Orai1 Abundance Determination by Flow Cytometry

After 36 hours of transfection, siControl, siRap1A, and siRap1A+siOrai1 (2 nmol/L) transfected cells were lifted by Trypsin-EDTA, washed with PBS, and incubated with 7-aminoactinomycin D for 30 minutes on ice in the dark. For surface staining, ECs were incubated for 60 minutes at 37 °C with anti-Orai1 primary antibody (1:200; Abcam; No. ab111960), followed by 488A-labeled anti-rabbit secondary antibody (1:250; Cell Signaling Technology; No. 4412) for 30 minutes (37 °C). The cells were washed, resuspended with FACS (fluorescence-activated cell sorting) buffer, and analyzed using the FACS Calibur flow cytometer (BD Biosciences).

Analysis of NFAT Nuclear Translocation by Confocal Microscopy

hMVECs were plated onto fibronectin-coated (2.5 µg/mL) coverslips in a 6-well plate at a density of 3×10^5 cells per well and transfected with 50 nmol/L Rap1A siGENOME siRNA pool or with nontargeting siRNA pool (Dharmacon) for 6 hours in the OPTIMEM media. Cells were then cultured in complete EGM-2 MV culture medium. After 30 hours, siControl and siRap1A cells were stimulated with thrombin (1 U/mL) for 20 minutes in the presence of 2 mmol/L Ca^{2+} in the media. For NFAT inhibition, hMVECs were pretreated in the ECs with calcineurin inhibitor (FK-506; 1 µmol/L; diluted in 10% dimethyl sulfoxide) 30 minutes before thrombin stimulation. After stimulation, ECs were fixed in 4% paraformaldehyde and permeabilized using 0.3% Triton X-100. Then, coverslips were blocked with 5% BSA and stained overnight at 4 °C with an anti-NFAT1 antibody (1:50; Cell Signaling Technology; No. 4389S), followed by rabbit secondary antibody conjugated with Alexa Fluor 488 (1:1000; Cell Signaling Technology; No. 4412) for 2 hours at room temperature. DAPI (4′,6-diamidino-2-phenylindole) and phalloidin Texas Red (Invitrogen; No. T7471) were used to stain nuclei and cytoskeleton, respectively. Fluorescent images were acquired with a Zeiss laser scanning confocal microscope using the 100× objective lenses. NFAT1 nuclear translocation was measured by determining the nucleus-to-cytosolic ratio of the NFAT fluorescence intensity. Quantitation for each condition was performed by counting cells in 5 randomly chosen fields (a total of 15 cells per group).

NFAT Luciferase Activity

hMVECs were transfected with siRNA targeting Rap1A, Orai1, or a nontargeting control using lipofectamine 2000. After 24 hours, these cells were further transfected with a Renilla luciferase plasmid (pRL TK; Promega; No. E2241) alone or together with a plasmid encoding NFAT luciferase reporter (Addgene; No. 10959). Following an additional 24 hours, cells were exposed to 1 U/mL thrombin for 20 minutes. NFAT activity was assessed in cell lysates using a (firefly) Luciferase assay with the Dual-Luciferase Reporter Assay Kit (Promega; No. E2920) and then normalized to Renilla luciferase activity.

Cytokine Array

Proinflammatory cytokines in supernatants of siControl and siRap1A hMVECs were detected using a Proteome Profiler Human Cytokine Array kit (R&D Systems, Inc; catalog No. ARY005B), following the manufacturer's protocol. Supernatants of siControl and siRap1A hMVECs were collected after 36 hours of siRNA transfection and pooled, with 3 replicates per condition, and incubated with human cytokine array membrane. The chemiluminescence signal intensities were detected using Amersham Imager 680 (GE Health Care). Densitometry was performed with the Image J software.

Animal Model

All mouse procedures were performed according to the Medical College of Wisconsin Institutional Animal Use and Care Committee. Generation of EC-specific Rap1A-knockout mice (Cadh5[PAC]-CreERT2$^{+/0}$; Rap1A$^{f/f}$ Rap1B$^{+/+}$; Rap1A$^{i\Delta EC}$) on the C57Bl/6J background was previously described.[51] We used both male and female mice. Animals were fed the PicoLab laboratory rodent diet 5L0D containing crude protein (23%), crude fat (4.5%), and crude fiber (6%). Tamoxifen in peanut oil (100 µg IP) was injected into 1-week-old postnatal mice for 5 consecutive days to generate inducible Rap1A$^{i\Delta EC}$ mice, in which Rap1A is deleted in ECs. Cadh5-Cre-negative mice, or mice injected with

carrier oil only, were used as controls. The data from each sex were first analyzed separately for each condition to determine whether sex was a determinant in the context of experiments. We found there was no difference between sex groups, and the data for males and females were combined to improve power.

Lipid Nanoparticle siOrai1 Preparation and Treatment

siRNA sequences targeting Orai1 (siOrai1) were designed, and an siRNA targeting luciferase was used as a negative control (siLuc). siRNA sequences were synthesized by Integrated DNA Therapeutics and encapsulated in lipid nanoparticle (LNP) as previously described.[59] Briefly, siRNAs were dissolved in sodium acetate (pH 4) and combined with a lipid solution at an amine-to-phosphate ratio of 3. The LNP consisted of an ionizable cationic lipid, ALC-0315, and 3 helper lipids: cholesterol, DSPC (distearoylphosphatidylcholine), and PEG-DMG (1,2-dimyristoyl-rac-glycero-3-methoxypolyethylene glycol-2000) at a 50:38.5:10:1.5% molar ratio (Avanti Lipids). The LNPs were dialyzed against Dulbecco PBS at pH 7.4 in 500-fold volume excess. Cholesterol content was measured using the Cholesterol E Assay Kit (Wako Chemicals, Mountain View, CA), and RiboGreen assay (Quant-IT Ribogreen RNA Assay Kit; Thermo Fisher) was performed to determine mRNA concentration and encapsulation efficiency. siRNA-LNPs were diluted to 0.5 mg/mL in PBS (pH 7.4) and stored at 4 °C before injection. Mice were injected with LNP-siOrai1 and LNP-siLuc with 5 mg siRNA per kg body weight (mg/kg). A dose of 1 mg/kg siRNA is standard for inducing knockdown of mRNAs expressed in hepatocytes using siRNA-LNPs in mice, but the higher dose (5 mg/kg) applied in these experiments was used to ensure a greater biodistribution to target the endothelium.[60] Seven days post-injection, mice were euthanized, and the lungs were collected.

BAL Collection

Mice were anesthetized, and dissection was performed to expose trachea. An 18-mm gauze catheter was inserted into the trachea and knotted with suture tightly. One milliliter PBS was gently injected into the lung, aspirate was collected in a 15-mL tube and centrifuged the BAL (bronchoalveolar lavage) at 2000 rpm, 4 °C for 10 minutes. Supernatant was collected and protein content was estimated using the Pierce BCA protein assay kit (catalog No. 23227; Thermo Scientific). The remaining cell pellet was suspended in PBS, and cell count was performed using hemocytometer. IL-6 (interleukin-6) concentrations were determined using mouse IL-6 ELISA kit (catalog No. DY406-05; R&D Systems). Twelve Rap1A$^{i\Delta EC}$ mice and 6 littermate controls were used for analysis. Among 12 Rap1A$^{i\Delta EC}$ mice, 6 Rap1A$^{i\Delta EC}$ mice received siLuc LNP and other 6 Rap1A$^{i\Delta EC}$ mice received siOrai1 LNP.

Measurement of Pulmonary Edema

Mice were anesthetized, and dissection was performed to expose the trachea. The lung wet-to-dry ratio was used to evaluate the severity of pulmonary edema.[61,62] The lungs were removed, and the wet weight measured. The lungs were then placed in an incubator at 65 °C for 72 hours and the dry weight obtained. Twenty Rap1A$^{i\Delta EC}$ mice and 10 littermate controls were used for analysis. Among 20 Rap1A$^{i\Delta EC}$ mice, 10 Rap1A$^{i\Delta EC}$ mice received siLuc LNP and other 10 Rap1A$^{i\Delta EC}$ mice received siOrai1 LNP.

Isolation of Primary Mouse Lung ECs and Analysis of Myeloid Cell Populations

Mice were anesthetized using ketamine (100 mg/kg IP) and xylazine (10 mg/kg IP). Twelve Rap1A$^{i\Delta EC}$ mice and 6 littermate controls were used for analysis. Among 12 Rap1A$^{i\Delta EC}$ mice, 6 Rap1A$^{i\Delta EC}$ mice received siLuc LNP and other 6 Rap1A$^{i\Delta EC}$ mice received siOrai1 LNP. Mouse lung ECs were isolated from WT_siLuc LNP, Rap1A$^{i\Delta EC}$ mice_siLuc LNP, and Rap1A$^{i\Delta EC}$ mice_siOrai1 LNP groups of mice as we previously described.[63] Briefly, lung tissues were cut into small pieces using surgical scissors and digested with collagenase A (5 mL, 1 mg/mL) for 30 minutes at 37 °C. The tissue suspension was filtered through a 70-µm cell strainer (Falcon) and centrifuged (400*g*, 5 minutes) at room temperature to obtain a cell pellet. The cell pellet was resuspended in 3 mL of 0.1% BSA/PBS and incubated with anti-mouse CD31 antibody–conjugated Dynabeads at room temperature for 12 minutes. After bead incubation was complete, the cell suspension was mounted on the magnetic particle concentrator to isolate lung ECs, while the resulting supernatant was used for the analysis of myeloid cell frequency by flow cytometry. Trypan blue was used to count cells, and live/dead staining was performed using 7-aminoactinomycin D. Approximately 1×10^6 cells were fixed with 1.5% paraformaldehyde and subjected to a 6-color staining procedure at a 1:100 dilution. The following antibodies were used to identify myeloid cells in the lung tissue: CD45-APC/Cy7, Ly6C-FITC, Ly6G-PE, CD11b-BV605, F4/80-PE/Cy7, and Gr1-APC. The collected flow cytometry data were analyzed using the FACS Calibur flow cytometer (BD Biosciences).

Electrical Cell Impedance Sensing

EC barrier function was measured using ECIS in early passage hMVECs transfected with 50 nmol/L pooled siRNAs for 36 hours. The cells were seeded onto fibronectin-coated (5 µg/mL) 8W10E$^+$ ECIS arrays (Applied Biophysics, MA) and allowed to reach confluency before being treated with thrombin at 0.5 U/mL. After 24 hours of siRap1A knockdown, the ECs were further transfected with 2 nmol/L Orai1 siRNA and cultured for an additional 12 hours before barrier function assessment. The ECIS readings were analyzed at an alternating current frequency of 4000 Hz, which is commonly used to assess changes in barrier performance. The baseline barrier was measured and set for a minimum of 60 minutes using the multiple frequency/time setting, and the behavior of cell impedance (Z, Rb) was monitored using the ECIS-1600 R system (Applied Biophysics, Troy, NY).[46] hMVECs were exposed to the thrombin (0.5 U/mL) and the impedance data for each well recorded at 40-s intervals during the whole analysis period. The impedance data were normalized (Z′) by dividing the impedance values after adding test compounds by the impedance values before adding the compounds, using the following formula: Z′(t)=Zsample(t)/Zsample(t0). The term Zsample(t0) represents the impedance magnitude right before introducing test chemicals to the cell population.

Statistical Analysis

Statistical analyses were performed using R, version 4.3.2 (R Foundation for Statistical Computing), and GraphPad Prism,

version 9.5.1 (GraphPad Software). Graphs were generated using GraphPad Prism, version 9.5.1, and graphs represent mean values and SD. Data were assessed for normal distribution and homoscedasticity using the Levine test. The Student *t* test with Welch correction was used to measure statistical significance between 2 groups. For comparisons of >2 groups, 1-way ANOVA and 2-way ANOVA with Tukey multiple comparisons post hoc test were used. When data were not normally distributed, the Mann-Whitney *U* test or Wilcoxon rank-sum test was used to test whether there was a significant difference between 2 groups. For comparisons involving ≥3 groups, the Kruskal-Wallis test was used to calculate the overall *P* value. If the overall *P* value was significant, indicating that at least 2 groups differed significantly, post hoc pairwise comparisons were conducted using the Wilcoxon rank-sum test, with the Bonferroni correction applied to address the issue of multiple testing. In cases when the sample size was too small to perform the Wilcoxon rank-sum test, the Welch 2-sample *t* test was used for comparing siControl and siRap1A, accounting for unequal variances among the groups. All statistical tests were 2 sided, and a *P* value of <0.05 was considered statistically significant.

RESULTS

Rap1A Restricts Agonist-Induced Ca^{2+} Influx

To determine the potential contribution of Rap1 to the regulation of Ca^{2+} signaling in hCAECs, we examined the effect of Rap1 knockdown with siRNA on ATP-evoked Ca^{2+} mobilization in hCAECs loaded with 2 µmol/L Fura-2 AM, a ratiometric Ca^{2+} indicator. ATP acts via the purinergic receptor (P2Y), a GPCR that couples to PLCβ (phospholipase Cβ) activation, and inositol 1,4,5-triphosphate–mediated Ca^{2+} release from the ER stores. In control ECs transfected with a control siRNA (siControl) and bathed in nominally Ca^{2+}-free external solutions, ATP induced a significant Ca^{2+} release from the ER followed by a relatively modest Ca^{2+} influx across the plasma membrane when 2 mmol/L Ca^{2+} was restored to the extracellular bath solution (Figure 1A). Knockdown of Rap1A and Rap1B with a pan siRNA (siRap1) resulted in a small decrease in Ca^{2+} release compared with siControl cells (2.99±1.06 versus 3.14±1.32, respectively). However, subsequent Ca^{2+} entry was significantly increased in siRap1A versus siControl hCAECs (2.77±1.34 versus 1.07±0.36; Figure 1A). To determine that this effect of siRap1 on Ca^{2+} entry is specifically mediated through SOCE, we used thapsigargin, a specific inhibitor of the SERCA (sarcoplasmic/ER Ca^{2+}-ATPase), which triggers SOCE through passive store depletion, bypassing inositol 1,4,5-triphosphate production.[64] SERCAs are evolutionarily ancient Ca^{2+} pumps located in the ER/AR and expressed by all cells, including ECs. SERCA proteins are the products of 3 genes, of which SERCA2a and SERCA3 are expressed in ECs,[65–67] whereas SERCA2b is the principal isoform in the smooth muscle.[65] While thapsigargin induced Ca^{2+} entry in both siControl ECs and siRap1 ECs, Ca^{2+} entry was significantly higher in hCAECs with Rap1 knockdown versus siControl (5.01±0.80 versus 2.51±0.32, respectively; Figure 1B). These findings demonstrate that while Rap1 knockdown leads to a small reduction in Ca^{2+} release from the ER, it significantly enhances agonist-induced SOCE.

Two Rap1 isoforms are expressed in ECs, Rap1A and Rap1B, which share 95% amino acid sequence identity, yet have a differential effect on Ca^{2+}-dependent signaling in ECs.[52] While Rap1B is the predominant isoform,[46] Rap1A uniquely mitigates Ca^{2+}-dependent signaling.[52] To understand the isoform-specific roles of Rap1 in SOCE, we determined the effects of siRNA specifically targeting the Rap1A isoform (siRap1A; Figure S1A) on Ca^{2+} mobilization in ECs in response to thapsigargin. Similar to the results obtained with pan siRap1 knockdown (Figure 1B), specific knockdown of the Rap1A isoform alone potentiated thapsigargin-induced SOCE compared with siControl (Figure 1C). Interestingly, specific knockdown of the more predominant Rap1B isoform did not alter SOCE (Figure 1C; Figure S1B). These data suggest that the Rap1A isoform uniquely and specifically restricts SOCE in hCAECs.

Enhanced SOCE by Rap1A Knockdown Is Inhibited With Classical CRAC Channel Blockers

To determine whether the upregulated store depletion–induced Ca^{2+} entry upon knockdown of Rap1A is mediated by CRAC channels encoded by Orai proteins, we examined the impact of 2 widely used CRAC channel inhibitors, GSK-7975A and BTP2.[68] 10 µmol/L BTP2 and 10 µmol/L GSK-7975A blocked thapsigargin-induced Ca^{2+} influx in both siControl and siRap1A ECs (Figure 2A and 2B), suggesting that this Ca^{2+} entry is indeed mediated by SOCE and Orai channels. We also examined the ability of low concentration of the lanthanide, gadolinium (5 µmol/L Gd^{3+}), to inhibit SOCE. At this relatively low concentration, Gd^{3+} is a specific Orai channel inhibitor.[68] We found that Ca^{2+} influx was blocked by 5 µmol/L Gd^{3+} in response to physiological and pharmacological stimulation with thrombin and thapsigargin, respectively (Figure 2C and 2D), further implicating Orai1 channels in this pathway.

Rap1A Knockdown Leads to Enhanced CRAC Channel Current Density in ECs

To provide biophysical evidence that Orai channel activity is indeed increased in response to Rap1A silencing, we transfected hCAECs with either siControl or siRap1A and measured I_{CRAC} using the whole-cell patch clamp technique as described previously.[12,68,69] After break-in, ER Ca^{2+} store depletion necessary to

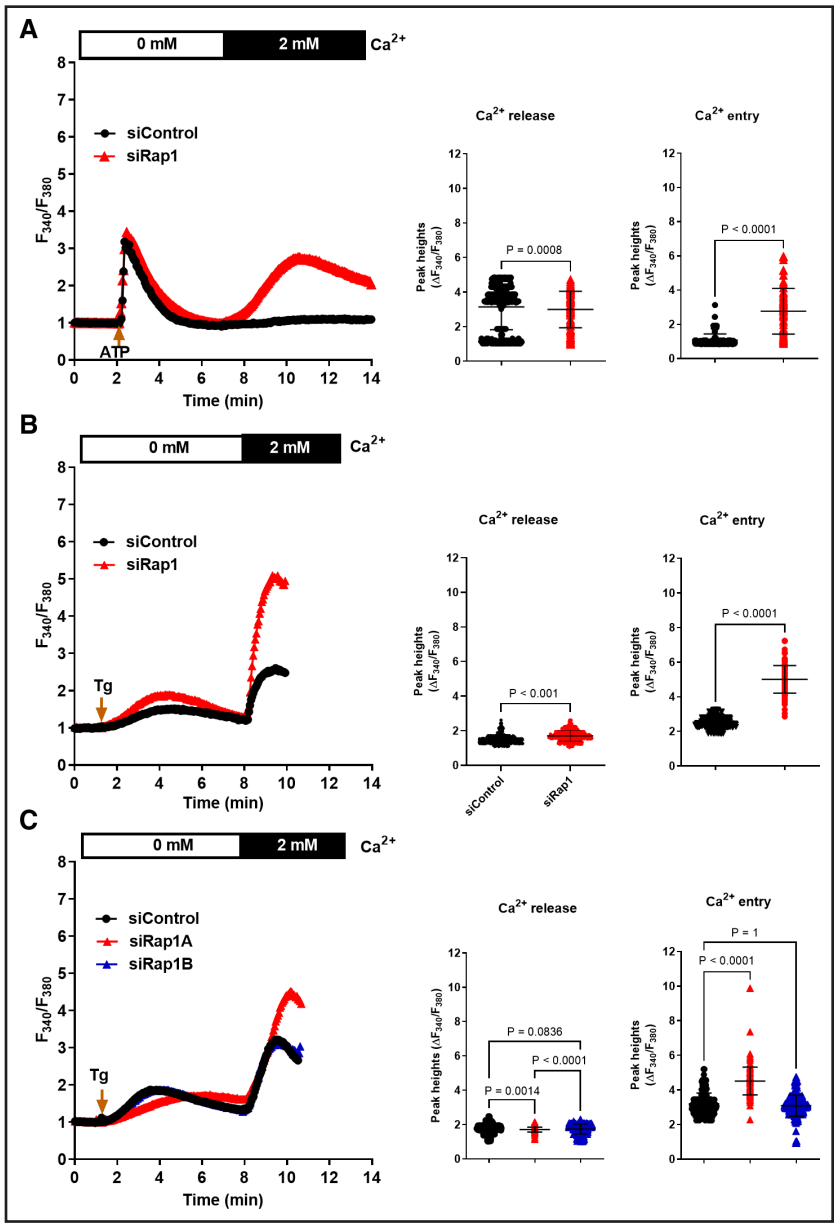

Figure 1. Rap1A (Ras-proximate-1) restricts agonist-induced Ca^{2+} influx in human coronary artery endothelial cells (hCAECs).
A, Elevated ATP-induced Ca^{2+} entry and slightly decreased Ca^{2+} release in siRap1A hCAECs. **B**, Rap1 limits thapsigargin (Tg)-induced Ca^{2+} entry in hCAECs. **C**, Rap1A, but not Rap1B, limits Tg-induced Ca^{2+} entry in hCAECs. **Left**, Representative fluorescence 340/380 ratio plots of individual hCAECs loaded with Fura-2/AM (Fura-2-acetoxymethyl ester) Ca^{2+} indicator and stimulated with 500 µmol/L ATP or 250 nM Tg in the absence and presence of 2 mmol/L external Ca^{2+}. **Right**, Maximum fluorescence ratios for Ca^{2+} release and Ca^{2+} entry were plotted. Statistical analysis was performed using the Wilcoxon rank-sum test. **C**, Bonferroni correction applied to address the issue of multiple comparison (n=150 cells per experiment; 3 independent experiments).

activate I_{CRAC} is induced by dialysis of cells through the patch pipette with a solution containing 20 mmol/L BAPTA. Currents are elicited by voltage ramps from −150 to +50 mV from a holding potential of 0 mV (Figure 3A and 3B). Due to the small size of native I_{CRAC}, in ECs in particular,[12] we used short pulses of divalent-free bath solutions to allow Na^+ ions to permeate through CRAC channels, hence amplifying the current. This results in an inward Na^+ I_{CRAC} in both siControl and siRap1A ECs that shows the typical depotentiation in divalent-free solutions (Figure 3C through 3F) with inwardly rectifying current/voltage relationship (Figure 3G). The current/voltage curves show that I_{CRAC} current density (pA/pF) increases by ≈3-fold after Rap1A silencing in hCAECs (hCAEC siControl: 2.33±0.56 pA/pF versus hCAEC siRap1a: 6.07±1.67 pA/pF; Figure 3G and 3H). Thus, Rap1A controls CRAC current density in ECs.

Partial Knockdown of Orai1 Rescues the Enhanced Ca^{2+} Entry in siRap1A ECs

The increased SOCE observed in siRap1A hCAECs was effectively inhibited by Orai1 inhibitors (Figure 2A through 2C), indicating a modulatory role of Rap1A on Orai1 channels. Furthermore, direct measurement of CRAC currents demonstrated increased CRAC current density (Figure 3G and 3H). To determine whether increased Orai1 channel expression may be responsible for increased Ca^{2+} entry in the absence of Rap1A, we measured Orai1 mRNA and protein abundance in siRap1A and siControl hCAECs. Orai1 mRNA expression

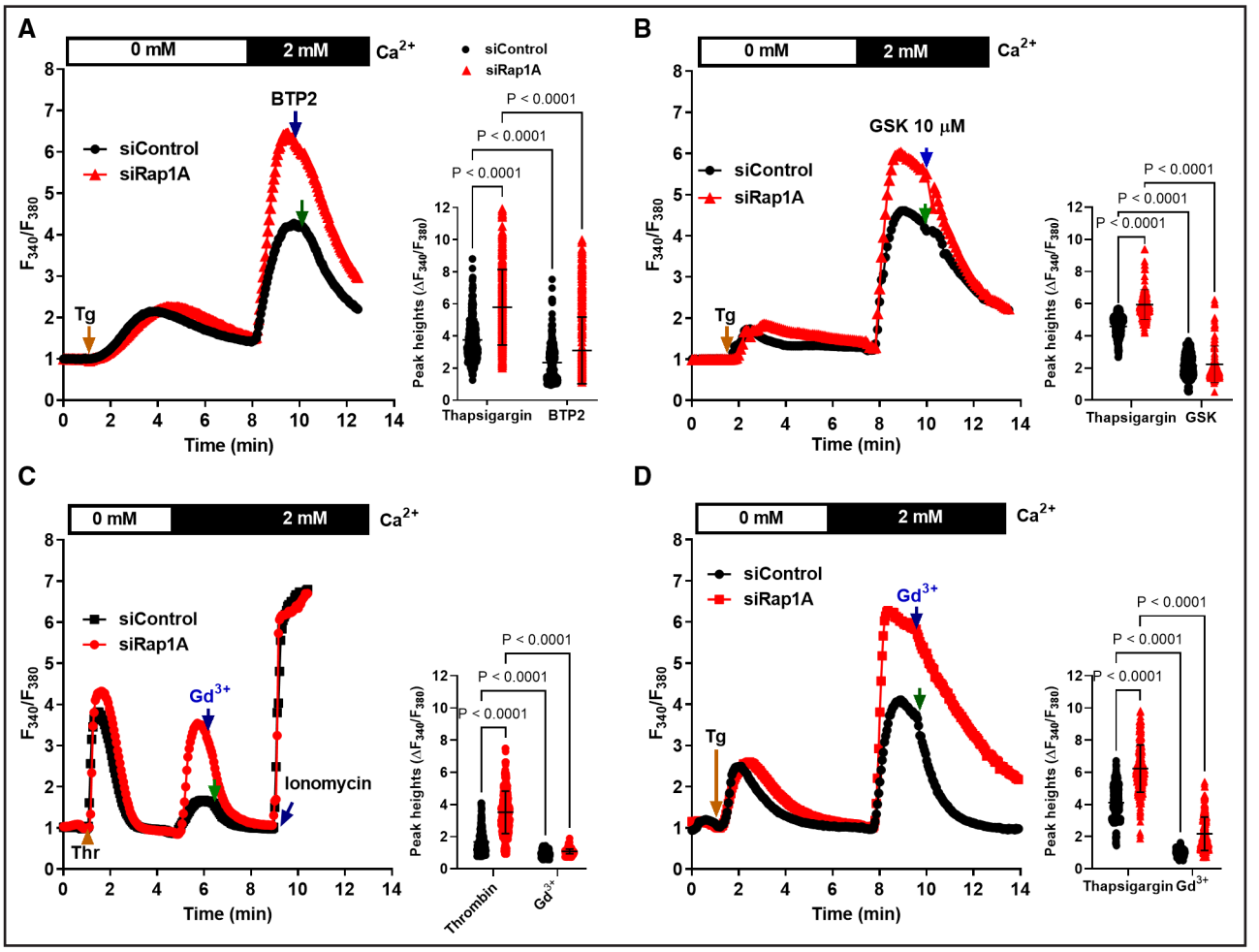

Figure 2. Rap1A (Ras-proximate-1) controls Orai1 (calcium release-activated calcium modulator 1) activity.
A through **C**, siRap1A-induced increase in store-operated calcium entry (SOCE) is sensitive to Orai1 inhibitors: (**A**) 10 μmol/L BTP2 (N-[4-[3,5-bis(trifluoromethyl)-1H-pyrazol-1-yl]phenyl]-4-methyl-1,2,3-thiadiazole-5-carboxamide), (**B**) 10 μmol/L GSK-7975A, and (**C** and **D**) 5 μmol/L Gd^{3+}. Inhibitors were introduced at the peak of Ca^{2+} entry to suppress it. Ca^{2+} fluorescence measurements in individual siControl and siRap1A human coronary artery endothelial cells (hCAECs) stimulated with 250 nmol/L Tg or 1 U/mL thrombin were performed as in Figure 1. Maximum fluorescence ratios were plotted. The Kruskal-Wallis test was used to calculate the overall *P* value and, the post hoc pairwise comparisons were conducted using the Wilcoxon rank-sum test, with the Bonferroni correction for multiple comparison (n=100 cells per experiment; 3 independent experiments).

was significantly increased in the absence of Rap1A (Figure 4A; Figure S1A). We next measured protein expression of the 2 Orai1 isoforms, the 33-kDa Orai1α and the 23-kDa Orai1β, that arise from alternative translation initiation from methionine 64 in Orai1α. Both isoforms of Orai1 are functionally similar and support SOCE and CRAC current (I_{crac}).[70,71] The analysis of total cellular protein by Western blotting revealed that the expression of Orai1 α and β isoforms was elevated in siRap1A hCAECs compared with siControl hCAECs (Figure 4B). Densitometry measurements indicate lower total Rap1 content in siRap1A ECs (0.62±0.08 Rap1/actin) versus siControl (0.79 Rap1/actin), indicating Rap1A knockdown (Figure 4B). We expect only a small change in total Rap1, as Rap1A is the less dominant Rap1 isoform in ECs.[46] Flow cytometry analysis of surface protein expression also revealed elevated levels of Orai1 in siRap1A versus siControl hCAECs (Figure 4C). Therefore, it is likely that enhanced Orai1 expression is responsible for increased SOCE in Rap1A-deficient hCAECs.

To examine the physiological significance of increased Orai1 expression on enhanced Ca^{2+} entry in siRap1A hCAECs, we attempted a partial knockdown of Orai1 in siRap1A hCAECs to normalize Orai1 protein expression to control levels. We found that transfecting siRap1A hCAECs with 2 nmol/L of a pool of Orai1 siRNA (siOrai1) resulted in normalized Orai1 mRNA level in siRap1A hCAECs, comparable to siControl hCAECs (Figure 4A). Furthermore, this partial knockdown of Orai1 resulted in normalized Orai1 protein expression in siRap1A hCAECs (Figure 4B and 4C). Functionally, partial Orai1 knockdown in siRap1A ECs significantly reduced thapsigargin-induced SOCE in siRap1A hCAECs to levels near those observed in siControl hCAECs (Figure 4D). This result

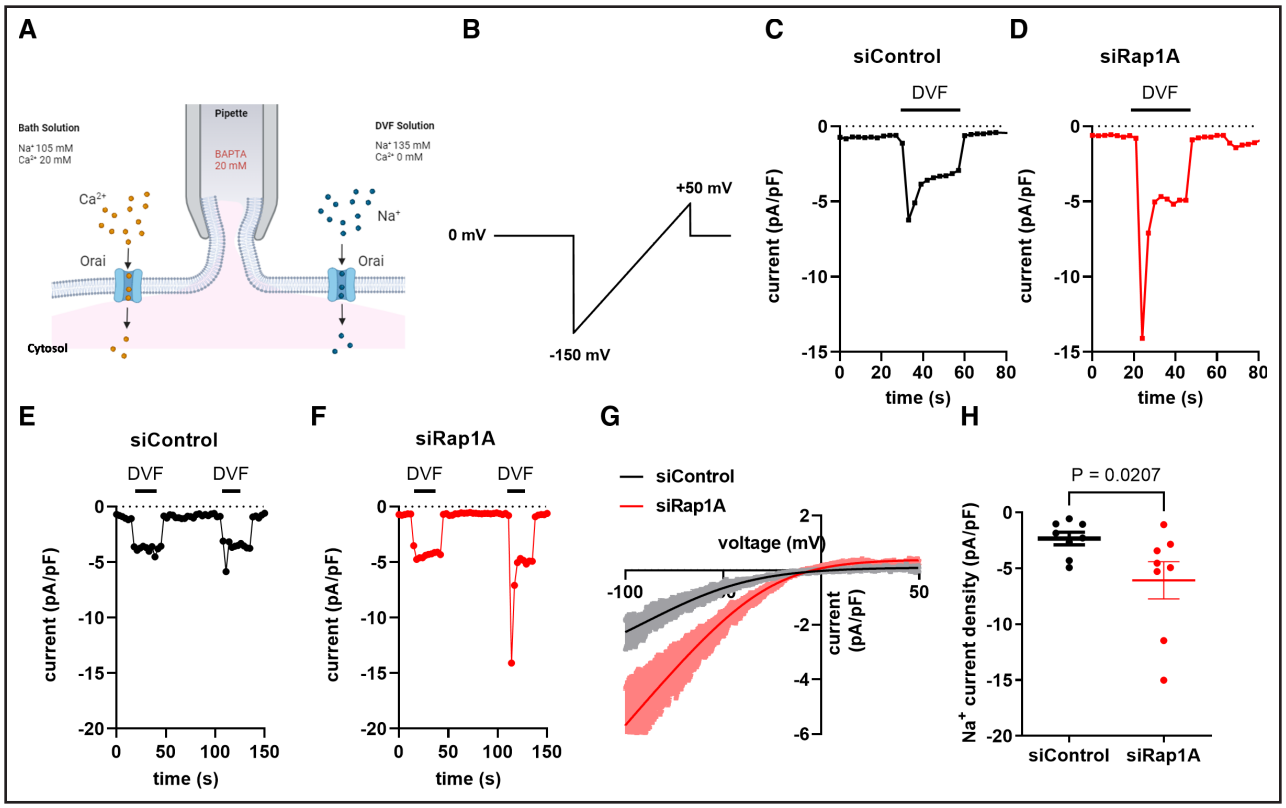

Figure 3. Rap1A (Ras-proximate-1) silencing increases Ca^{2+} release-activated Ca^{2+} (CRAC) current density in human coronary artery endothelial cells (hCAECs).

A, Whole-cell configuration of the patch clamp technique allowing the recording of I_{CRAC}. After break-in with a pipette solution containing 20 mmol/L BAPTA (1,2-bis(o-aminophenoxy)ethane-N,N,N′,N′-tetraacetic acid) to deplete the endoplasmic reticulum (ER) stores and activate Orai (calcium release-activated calcium modulator 1) channels, I_{CRAC} develops. This current is small, which necessitated current amplification through the use of pulses of divalent-free (DVF) solutions. This Na^+ I_{CRAC} shows the typical depotentiation in DVF solutions. **B**, Voltage ramp protocol used to measure I_{CRAC} in hCAECs after dialysis with 20 mmol/L BAPTA in the patch pipette solution to deplete the ER stores. **C**, and **D**, Representative current measured in DVF solutions at −100 mV in hCAECs transfected with either siControl or siRap1a for 48 hours. **E**, and **F**, Time course of I_{CRAC} activation in hCAECs transfected with either siControl or siRap1A taken at −100 mV in DVF solutions. **G**, Representative I-V curves of Na^+ I_{CRAC}, in hCAECs transfected with either siControl or siRap1a. **H**, Na^+ I_{CRAC} density measured at −100 mV in both hCAEC siControl (n=8) and hCAEC siRap1a (n=8; Mann-Whitney *U* test; *P*=0.021).

suggests that Rap1A restricts agonist-induced SOCE through inhibiting *Orai1* gene expression.

Rap1A Restricts Thrombin-Induced NFAT Activation in hMVECs

Elevated SOCE in siRap1A ECs led us to investigate the activation of nuclear factor of activated T cells (NFAT), a Ca^{2+}-sensitive transcription factor specifically activated downstream CRAC/Orai1 channel activity in nonexcitable cells. The activity and nuclear translocation of NFAT are regulated by its phosphorylation status. Phosphorylated NFAT under basal conditions is localized in the cytoplasm. Increased Ca^{2+} levels through enhanced SOCE activity cause the activation of the phosphatase calcineurin (calmodulin-dependent serine/threonine phosphatase), which dephosphorylates NFAT, exposing a hidden nuclear localization signal and causing its nuclear translocation to control gene transcription.[26,72] hMVECs express all 5 isoforms of NFAT: NFAT1 (NFATc2), NFAT2 (NFATc1), NFAT3 (NFATc4), NFAT4 (NFATc3), and NFAT5 (NFATc5)[73] (Figure S2). Rap1A knockdown in ECs lead to increased expression of NFAT1, NFAT2, and NFAT4 (Figure S2). To determine whether enhanced SOCE in the absence of Rap1A in ECs leads to enhanced NFAT activation, we assessed NFAT nuclear translocation in siRap1A hMVECs in response to thrombin stimulation. Under basal conditions, native NFAT1 detected by immunofluorescence staining was found predominantly in the cytoplasm in siControl and siRap1A hMVECs (Figure 5A, top and fourth rows, respectively, and Figure 5B) with an average nuclear intensity of 0.00±0.353. Thrombin stimulation (1 U/mL, 20 minutes)–induced translocation of NFAT1 to the nucleus as determined by the fold increase of nuclear intensity is 1.0815±0.528 (Figure 5A, second row, and Figure 5B). Interestingly, thrombin-induced nuclear translocation of NFAT1 was significantly increased in siRap1A hMVECs compared with siControl hMVECs, with a fold change of 2.086±0.781 (Figure 5A, fifth

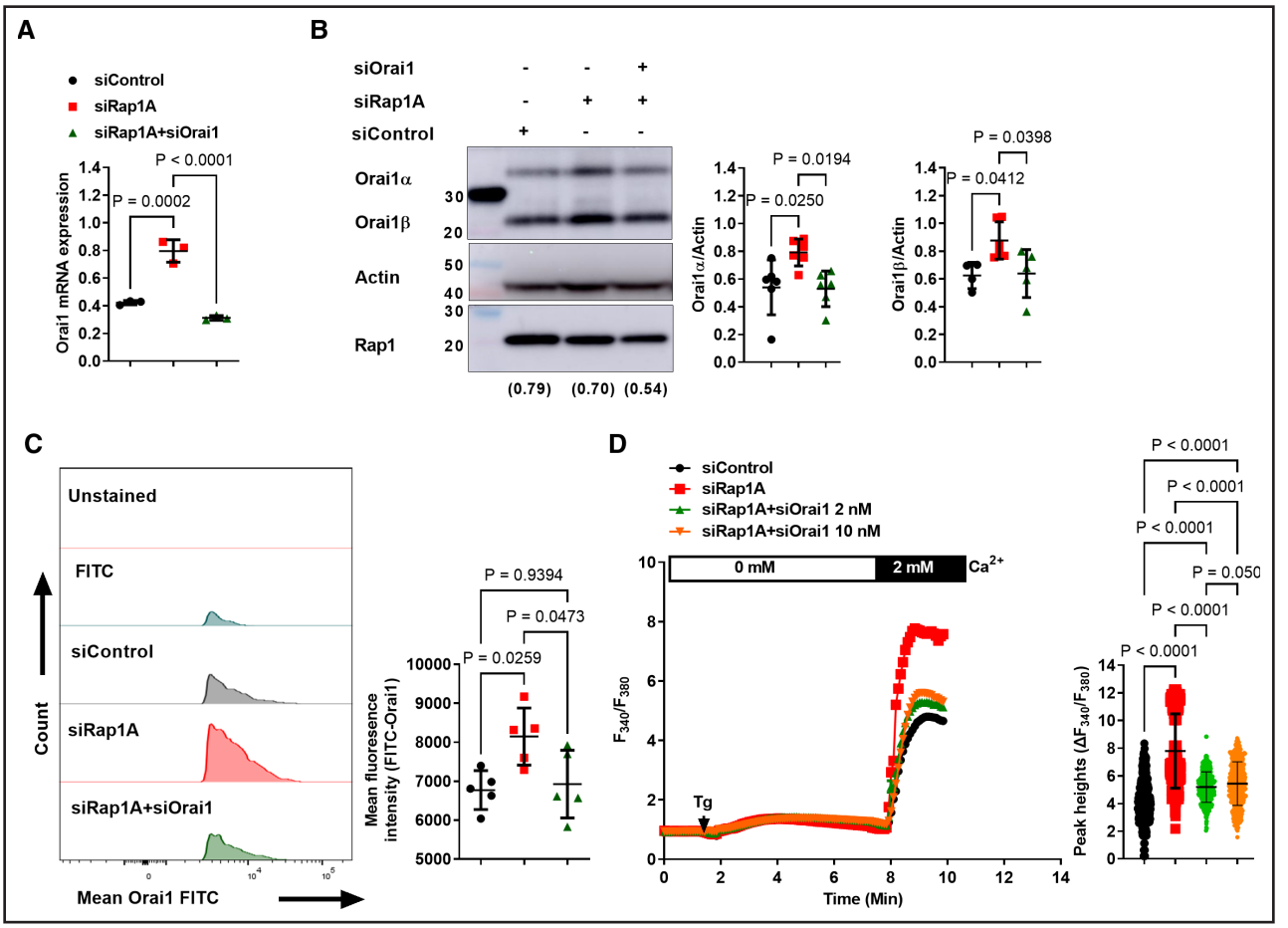

Figure 4. Partial knockdown of Orai1 (calcium release-activated calcium modulator 1) rescues excessive Ca^{2+} entry in siRap1A human coronary artery endothelial cells (hCAECs).

A, Enhanced *Orai1* gene and (**B** and **C**) protein expression in siRap1A hCAECs is normalized to siControl level by partial knockdown of Orai1 (2 nmol/L). **A**, qPCR (quantitative polymerase chain reaction) analysis (n=3 biological replicates). **B**, Representative Western blots and densitometry calculations of Orai1 normalized to actin were plotted (n=6 biological replicates). Densitometry values of Rap1 (Ras-proximate-1) normalized to actin were provided within the parenthesis. **C**, Histogram of cell surface Orai1 abundance measured by flow cytometry in siControl, siRap1A, and siRap1A+siOrai1 (2 nmol/L) hCAECs was plotted. Arithmetic mean of the surface Orai1 fluorescence intensity was compared between experimental groups (n=4 independent experiments). **D**, Ca^{2+} measurements in individual siControl and siRap1A hCAECs were performed as in Figure 1 (n=150 cells per experiment; 3 independent experiments). Statistical significance was measured using 1-way ANOVA with Tukey multiple comparisons post hoc test (**A**–**C**) and Kruskal-Wallis with Wilcoxon rank-sum post hoc test, with the Bonferroni correction for multiple comparison (**D**).

row, and Figure 5B). The calcineurin inhibitor FK-506 (1 μmol/L) effectively prevented the enhanced nuclear translocation of NFAT1 in both siControl and siRap1A hMVECs, reducing them to basal prethrombin stimulation levels (Figure 5A, sixth row, and Figure 5B). This finding indicates that Rap1A plays a role in inhibiting the calcineurin/NFAT pathway in ECs.

To gain further evidence that Rap1A suppresses NFAT activation in ECs, we used NFAT luciferase assay in siRap1A and siControl hMVECs. While under basal conditions NFAT activity was similar in siControl and siRap1A ECs, thrombin stimulation led to significantly increased NFAT activity in siRap1A hMVECs compared with siControl hMVECs, with a fold change of 1.55±0.081 (Figure 5D). The calcineurin inhibitor FK-506 effectively inhibited the enhanced NFAT luciferase activity in both siControl and siRap1A hMVECs (Figure 5D). Furthermore, partial knockdown of Orai1 in siRap1A hMVECs also effectively normalized the elevated NFAT activity to the control level (Figure 5E). Combined, these findings support the role of Rap1A in the suppression of NFAT activity by restricting Orai1 expression.

Rap1A Restricts NFAT-Mediated Proinflammatory Transcription in hMVECs

Activated NFAT, together with other transcription factors (eg, activator protein 1 [Fos/Jun]), drives the transcription of inflammatory cytokines.[72] Excessive NFAT activation is associated with inflammation in ECs.[74,75] The increased thrombin stimulated NFAT nuclear translocation in siRap1A hMVECs compared with siControl

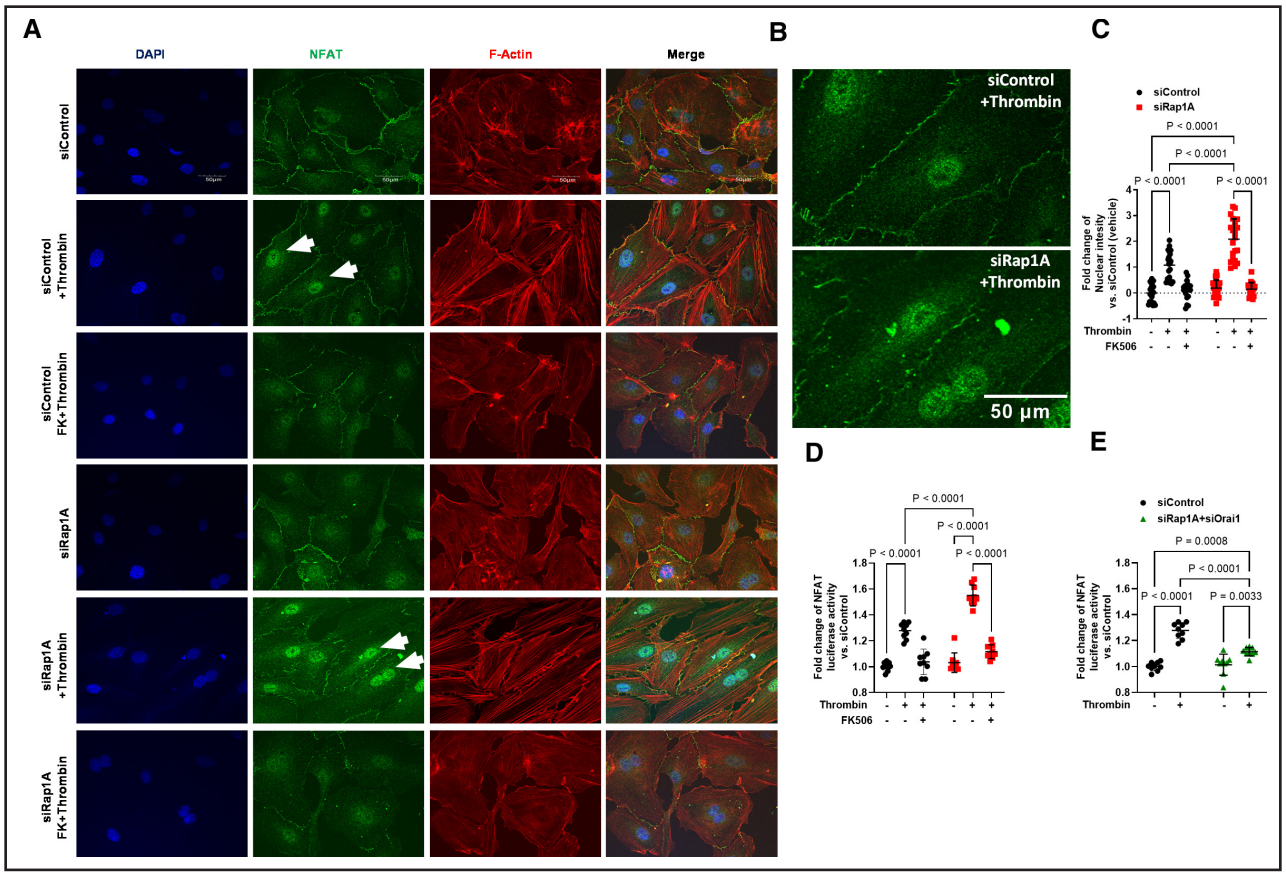

Figure 5. Rap1A (Ras-proximate-1) restricts thrombin-induced nuclear factor for activated T cells (NFAT) activity in human lung microvascular endothelial cells (hMVECs).

A, Confocal fluorescence microscopy images of NFAT in siControl and siRap1A hMVECs stimulated with thrombin (1 U/mL, 20 minutes) in the presence or absence of calcineurin inhibitor (FK-506). NFAT1 antibody (green), DAPI (4′,6-diamidino-2-phenylindole; blue), and phalloidin (Texas red) were used to stain NFAT1, nucleus, and actin cytoskeleton, respectively. Arrows indicate nuclear NFAT. **B**, Enlarged images indicated by arrows in **A**. **C**, Fold change of nuclear intensity of NFAT vs siControl is shown (n>15 independent experiments). **D**, Luciferase reporter assay in siControl and siRap1A transfected hMVECs treated with 1 U/mL thrombin in the presence or absence of FK-506 (n=9). **E**, Luciferase reporter assay in siControl and siRap1A+siOrai1 2 nM transfected hMVECs treated with or without 1 U/mL thrombin (n=9 biological replicates). Two-way ANOVA with Tukey multiple comparisons post hoc test was applied to measure the statistical significance.

hMVECs led us to hypothesize that the absence of Rap1A in ECs may enhance NFAT's proinflammatory transcription activity. Therefore, we used a cytokine array to measure the levels of cytokines in siControl and siRap1A hMVEC supernatants. While CCL2 (chemokine [C-C motif] ligand 2), a key cytokine involved in recruiting of monocytes/macrophages, was decreased in siRap1A ECs, other inflammatory cytokines, CCL5 (chemokine [C-C motif] ligand 5) and CXCL11 (C-X-C motif chemokine 11), were significantly upregulated in siRap1A supernatants compared with those from siControl hMVECs (Figure 6A and 6B). These results indicate that Rap1A deficiency may lead to an inflammatory state in ECs.

To confirm the inflammatory state in Rap1A-deficient ECs, we assessed the levels of the NFAT-dependent cytokine IL-6, a known marker of inflammation.[76] Thrombin, generated in response to vascular injury and inflammation, physiologically contributes to lung permeability and inflammation. Thrombin treatment (1 U/mL, 0–12 hours) induced IL-6 expression in both siControl and siRap1A hMVECs, with siRap1A hMVECs showing a significant elevation in IL-6 levels compared with siControl hMVECs after 12 hours of stimulation (Figure 6C). The increase in IL-6 expression was attenuated by the calcineurin inhibitor FK-506, (Figure 6D), indicating it is NFAT dependent and suggesting that Rap1A limits NFAT-mediated proinflammatory transcription in ECs.

Elevated Vascular Permeability in Rap1A-Deficient Pulmonary ECs Is Orai1 Dependent

Previous studies have proposed a link between dysregulated STIM1/Orai1 expression or SOCE and increased pulmonary endothelial permeability.[27,53,77–83] To explore the role of Orai1-dependent increase in SOCE in hMVECs with reduced Rap1A expression, we used ECIS

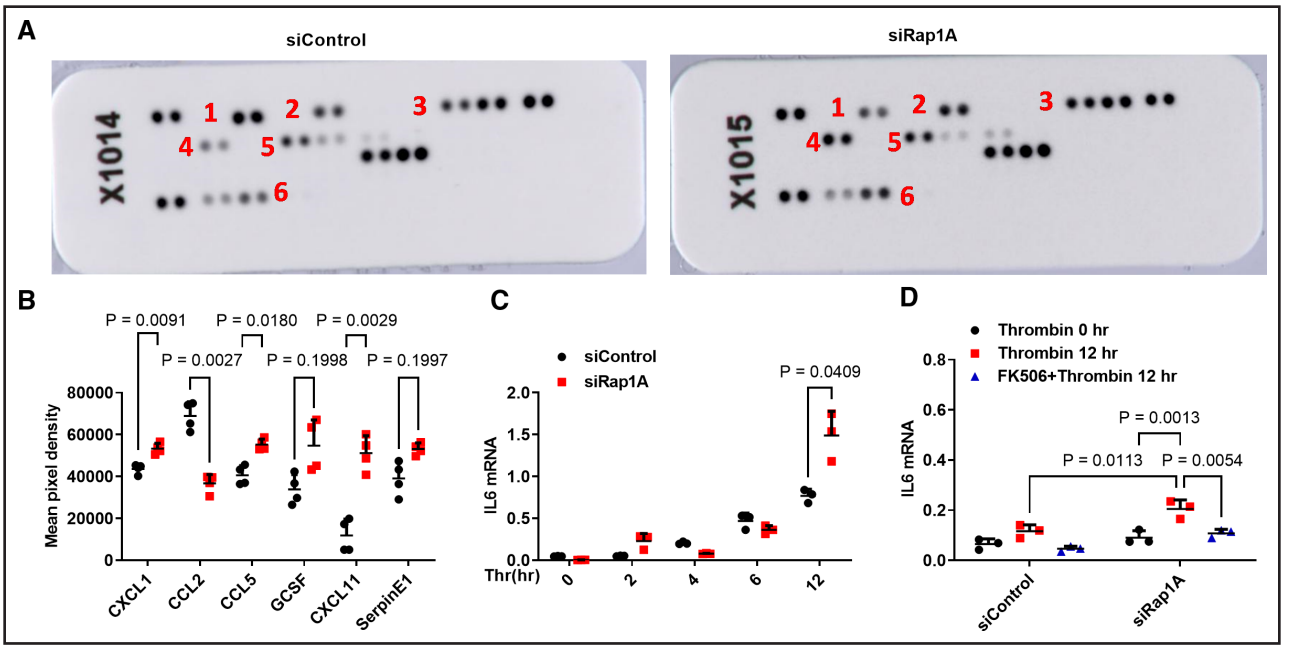

Figure 6. Elevated NFAT (nuclear factor for activated T cells)-dependent proinflammatory transcription in Rap1A (Ras-proximate-1)-deficient human lung microvascular endothelial cells (hMVECs).
A and **B**, Cytokine array profile of siControl and siRap1A hMVEC supernatants under basal conditions. **A**, Representative images of cytokine array. **B**, Densitometry values of indicated cytokines (n=2 independent experiments). **C** and **D**, Thrombin-induced IL (interleukin)-6 mRNA expression is NFAT dependent. **C**, Time course of thrombin-induced IL-6 expression. **D**, Analysis of gene expression of IL-6 in siControl and siRap1A hMVECs stimulated with thrombin for 12 hours in the presence or absence of FK-506 (n=3 biological replicates). Welch 2-sample *t* test with a Bonferroni correction for multiple testing (**B** and **C**) and 2-way ANOVA with Tukey multiple comparisons post hoc test (**D**) were applied to measure the statistical significance.

to measure EC cell-cell adhesion.[54,84] We compared monolayers of control ECs, Rap1A-deficient ECs, and Rap1A-deficient ECs with partial knockdown of Orai1. After thrombin exposure, we measured the resistance of cell-cell contacts to current flow (Rb). As expected, thrombin (0.5 U/mL) induced a rapid and reversible decrease in resistivity in siControl hMVECs, representing transient increased permeability in siControl hMVECs (Figure 7A, black dots). This response was amplified in Rap1A-deficient cells, aligning with responses to VEGF (vascular endothelial growth factor) observed in previous studies[46] (Figure 7A, red squares). Notably, normalizing Orai1 expression in siRap1A hMVECs mitigated the thrombin-induced permeability, suggesting a return toward normal permeability levels by normalizing Ca^{2+} entry and the Ca^{2+}-dependent inflammatory response (Figure 7A, green triangles).

In vivo, Rap1A deletion in ECs resulted in elevated lung wet/dry ratio, indicative of enhanced vascular permeability and subsequent pulmonary edema (Figure 7B). This finding aligns with our previous reports on increased permeability associated with Rap1A deletion.[46] To assess whether the in vivo Rap1A deletion mirrors the in vitro effect on Orai1 expression, we compared Orai1 levels in lung ECs from control and Rap1A$^{i\Delta EC}$ mice. Increased Orai1 transcript and protein levels were evident in the ECs from Rap1A$^{i\Delta EC}$ lungs (Figure 7C and 7D). Consequently, we used LNPs that have tropism for both liver and endothelium[59] containing siOrai1 (siOrai1-LNP) in Rap1A$^{i\Delta EC}$ mice to explore the physiological impact on the lung vascular barrier. Treatment with siOrai1-LNP effectively normalized Orai1 expression in Rap1A$^{i\Delta EC}$ mice (Figure 7C and 7D, green triangles) and reduced lung edema (Figure 7B, green triangles), indicating that Rap1A modulates the pulmonary vascular barrier both in vitro and in vivo by regulating Orai1 expression.

Normalizing Endothelial Orai1 Mitigates Inflammation in Rap1A$^{i\Delta EC}$ Mice

The proinflammatory phenotype in Rap1A-deficient ECs prompted an investigation into inflammatory markers in Rap1A$^{i\Delta EC}$ mice. We observed increased protein levels and cell counts (Figure 7E), as well as heightened IL-6 levels (Figure 7F), in the bronchoalveolar lavage fluid (BALF) in Rap1A$^{i\Delta EC}$ mice compared with controls. The BALF protein and lung wet/dry ratio alterations serve as functional indicators of EC activation associated with enhanced vascular permeability, which leads to the development of pulmonary lung edema.[85] This finding suggests that an elevated inflammatory phenotype, like that seen in vitro, is associated with increased vascular permeability in the lungs of Rap1A$^{i\Delta EC}$ mice.

We reasoned that this inflammation stems from enhanced SOCE-dependent overactivation of NFAT and increase in cytokine production in lung ECs. To test

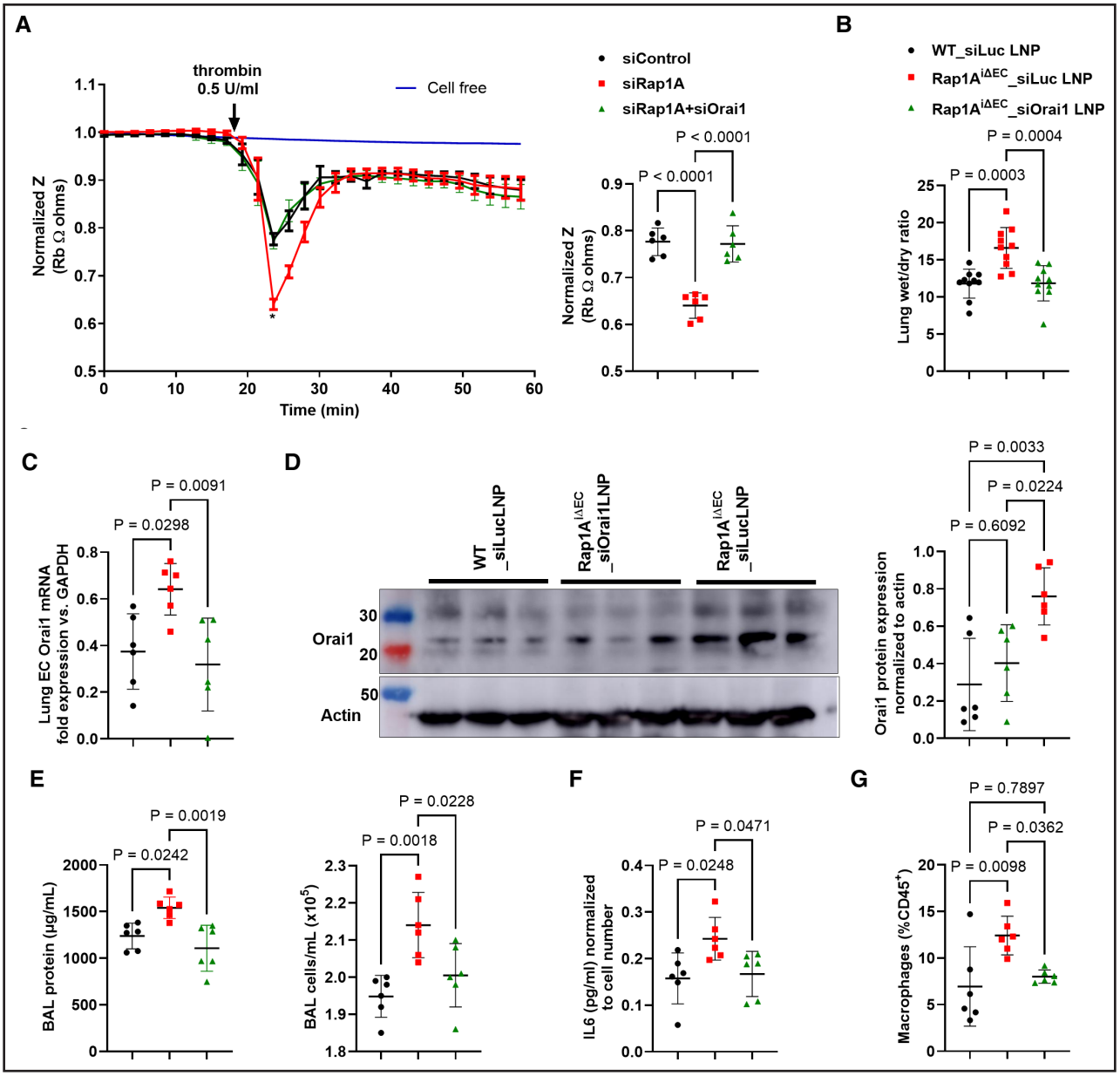

Figure 7. Elevated vascular permeability and inflammation in Rap1A (Ras-proximate-1)-deficient pulmonary endothelial cells (ECs) is Orai1 (calcium release-activated calcium modulator 1) dependent.

A, Normalizing Orai1 expression normalizes thrombin-induced permeability of Rap1A-deficient human lung microvascular endothelial cell (hMVEC) monolayers. EC barrier function was measured using electric cell-substrate impedance sensing (ECIS) at an alternating current frequency of 4000 Hz. The normalized impedance at the peak of barrier disruption (*) (z) is plotted (n=6 biological replicates). *P*<0.0001. **B** through **F**, siOrai1 delivery to lung ECs by lipid nanoparticles (LNPs) normalizes lung permeability and reduces inflammation in Rap1A$^{i\Delta EC}$ mice. **B**, Lung wet-to-dry ratio, a measure of pulmonary edema, in control and Rap1A$^{i\Delta EC}$ mice with or without siOrai1 LNP treatment (n=10 mice per each experimental group). Twenty Rap1A$^{i\Delta EC}$ mice and 10 littermate controls were used for analysis. Among 20 Rap1A$^{i\Delta EC}$ mice, 10 Rap1A$^{i\Delta EC}$ mice received siLuc LNP and other 6 Rap1A$^{i\Delta EC}$ mice received siOrai1 LNP. **C** and **D**, siOrai1-LNPs normalize Orai1 mRNA **C**, and protein expression **D**, in Rap1A$^{i\Delta EC}$ lung ECs to the control (wild-type [WT]) levels. RT-qPCR (reverse transcription polymerase chain reaction; **C**) and Western blot (**D**) analysis of *Orai1* gene expression in lung ECs from WT and Rap1A$^{i\Delta EC}$ in the presence or absence of LNP siOrai1 treatment (n=6 mice per each experimental group). Western blot densitometry calculations of Orai1 levels normalized to actin are plotted (**right**; n=6 mice per each experimental group). Twelve Rap1A$^{i\Delta EC}$ mice and 6 littermate controls were used for analysis. Among 12 Rap1A$^{i\Delta EC}$ mice, 6 Rap1A$^{i\Delta EC}$ mice received siLuc LNP and other 6 Rap1A$^{i\Delta EC}$ mice received siOrai1 LNP. **E** through **G**, Quantification of protein content and cell numbers. **E**, IL (interleukin)-6 abundance measured by ELISA (**F**) and macrophage numbers, represented as a percentage of CD45$^+$ cells, measured by flow cytometry (**G**) in BALF (bronchoalveolar lavage fluid) from control and Rap1A$^{i\Delta EC}$ mice with or without siOrai1 LNP treatment. IL-6 was determined by ELISA (n=6 mice per each experimental group). Twelve Rap1A$^{i\Delta EC}$ mice and 6 littermate controls were used for analysis. Among 12 Rap1A$^{i\Delta EC}$ mice, 6 Rap1A$^{i\Delta EC}$ mice received siLuc LNP and other 6 Rap1A$^{i\Delta EC}$ mice received siOrai1 LNP. One-way ANOVA with Tukey multiple comparisons post hoc test was applied to measure the statistical significance.

this, we examined the impact of LNP-siOrai1 treatment, which normalizes Orai1 expression (Figure 7C and 7D) on lung inflammation. Results showed that normalizing Orai1 expression led to a reduction in lung inflammation, as indicated by decreased BAL protein and cell content (Figure 7E, green dots), reduced IL-6 levels (Figure 7F) and a decrease in macrophage numbers in Rap1A$^{i\Delta EC}$ mice (Figure 7G). There were no significant differences between the groups in myeloid suppressor cells, monocytes, and neutrophils (Figure S3). These findings underscore the critical role of Rap1A in modulating lung inflammation and permeability through Orai1 expression regulation.

DISCUSSION

Our study reveals a crucial role of Rap1A in controlling endothelial Ca^{2+} homeostasis, thereby limiting inflammation. Specifically, we demonstrate that the Rap1A isoform of Rap1 uniquely regulates endothelial SOCE, thus maintaining EC Ca^{2+} balance. The distinctive control of SOCE by Rap1A is evidenced by enhanced CRAC current density in siRap1A ECs and the normalization of Ca^{2+} entry in siRap1A ECs using Orai1 channel blockers (5 µmol/L Gd^{3+}, 10 µmol/L BTP2, and 10 µmol/L GSK-7975A) or knockdown of Orai1 using siRNA. This regulation is critical, as Rap1A deficiency in pulmonary ECs results in increased SOCE, elevated NFAT activation, and augmented transcription of proinflammatory cytokines, particularly IL-6 in siRap1A ECs and BALF from Rap1$^{i\Delta EC}$ mice, suggesting a significant role in respiratory conditions like asthma and chronic obstructive pulmonary disease,[86,87] whose expression is regulated by NFAT.[31,76,88,89] Additionally, NFAT inhibition using FK-506 significantly reduced NFAT activity and IL-6 levels in siRap1A ECs to control levels. Normalizing Orai1 protein levels both in vitro and in vivo by LNP-mediated siOrai1 delivery effectively mitigates NFAT activity, lung inflammation, and hyperpermeability in Rap1A$^{i\Delta EC}$ mice. The study reveals a new regulatory role for the Rap1A-Orai1 signaling in maintaining pulmonary vascular barriers and controlling inflammation.

Complementing these insights, previous studies have highlighted Rap1's role in restoring lung endothelial barrier integrity and aiding recovery from acute lung injury,[90,91] emphasizing Rap1's effect on VE-cadherin and p120-catenin,[48,90] and particularly Rap1A's unique role[91] and its impact on proinflammatory signaling.[92] Earlier research focused on Rap1's adaptor function promoting VE-cadherin adhesion and cell-cell junction integrity that likely contributes to developmental barrier defects in EC-Rap1 KO mice.[44–47,93] The distinct function of Rap1A, especially in the pulmonary endothelium, as opposed to Rap1B,[46] suggests a significant interplay between Rap1A and Orai1 in protecting the pulmonary endothelial barrier. This model proposes that Rap1A limits Orai1 expression to regulate Ca^{2+} entry and EC permeability.

The STIM1/Orai1 pathway has been implicated in the maintenance of the vascular barrier under various pathological conditions.[94–100] Previous studies indicated that STIM1, but not Orai1, is required for thrombin-mediated dermal microvascular EC permeability.[53,83] One potential explanation for these seemingly opposite results is that Ca^{2+} entry through Orai1 itself does not contribute to thrombin-evoked EC permeability under control wild-type conditions but that the increase in Orai1 due to Rap1A loss causes hyperpermeability through inflammation. Alternatively, the effects of Orai1 on EC hyperpermeability could be specific to the lung over the systemic vasculature.

Using novel LNPs in an innovative therapeutic approach, we targeted elevated Orai1 expression in Rap1A-deficient pulmonary endothelium. This method effectively mitigated elevated SOCE, normalized endothelial permeability, and reduced both edema and inflammation in the lungs. The use of LNPs as a delivery mechanism enhances the specificity of the intervention, offering a promising therapeutic modality. These findings pave the way for further development in treating various lung diseases, leveraging the potential of targeting the Rap1A-Orai1 pathway to reverse endothelial dysfunction and alleviate pathological symptoms in pulmonary conditions.

While our study establishes that Rap1A restricts Orai1 expression to control SOCE and NFAT activity, the exact mechanism underlying Orai1 upregulation following Rap1A knockout remains elusive. This is in contrast to the NFAT5-mediated regulation of Orai in megakaryocytes,[101] as NFAT inhibition does not impede Orai1 upregulation in Rap1A KO, suggesting an alternative, non–NFAT-dependent pathway (R. Kosuru and M. Chrzanowska, unpublished data, 2023). In platelets, where Orai1 is crucial,[102,103] Orai1 expression is modulated by thrombin via translational mechanisms involving PI3K (phosphoinositide 3-kinase) and actin cytoskeleton, rather than transcriptionally.[104,105] However, our unpublished data indicate that thrombin does not modify Orai1 expression in ECs. The upregulation might be an indirect consequence of integrin activation, as integrins are known targets of Rap1.[44,106] For example, in asthma, integrin-β1 downregulation impacts Orai1, influencing airway smooth muscle and lung remodeling.[107] Altered integrin-ECM interactions, such as those with collagen,[108] might potentially lead to Orai1 overexpression. However, considering that both isoforms activate integrins in ECs,[109,110] this pathway might not be exclusive to Rap1A. Future research is needed to elucidate the transcriptional regulation mechanisms at play and determine whether Rap1A acutely controls Orai1 activity, thereby deepening our understanding of this critical signaling pathway.

In conclusion, our study contributes significant insights into the mechanism by which Rap1A modulates SOCE in the pulmonary endothelium. It highlights the essential role of Rap1A in maintaining endothelial barrier function

and restraining inflammation. The Rap1A-Orai1 signaling axis emerges as a promising therapeutic target for conditions associated with vascular permeability, including sepsis and acute lung injury. This discovery offers new avenues for targeting inflammation-induced hyperpermeability and related pathologies.

ARTICLE INFORMATION

Received June 28, 2024; accepted September 5, 2024.

Affiliations

Versiti Blood Research Institute, Milwaukee, WI (R.K., G.P.S., F.F., B.G.N., C.J.K., M.C.). Data Science Institute (K.Y.), Department of Pediatrics (T.M., A.M.), Department of Medicine (D.X.Z.), Department of Pharmacology and Toxicology (M.C.), and Cardiovascular Center (M.C.), Medical College of Wisconsin, Milwaukee. Department of Physiology and Biophysics, University of Illinois Chicago (P.H.G.). Department of Pharmacology and Chemical Biology (O.R., M.T.), Vascular Medicine Institute (M.T.), and UPMC Hillman Cancer Center (M.T.), University of Pittsburgh School of Medicine, PA.

Sources of Funding

This study was supported by the National Institutes of Health grant R01HL157893 (M. Chrzanowska and P.H. Goldspink).

Disclosures

None.

Supplemental Material

Table S1
Figures S1–S3
Major Resource Table

REFERENCES

1. Meghji J, Mortimer K, Agusti A, Allwood BW, Asher I, Bateman ED, Bissell K, Bolton CE, Bush A, Celli B, et al. Improving lung health in low-income and middle-income countries: from challenges to solutions. *Lancet*. 2021;397:928–940. doi: 10.1016/S0140-6736(21)00458-X
2. Ackermann M, Verleden SE, Kuehnel M, Haverich A, Welte T, Laenger F, Vanstapel A, Werlein C, Stark H, Tzankov A, et al. Pulmonary vascular endothelialitis, thrombosis, and angiogenesis in Covid-19. *N Engl J Med*. 2020;383:120–128. doi: 10.1056/NEJMoa2015432
3. Huertas A, Guignabert C, Barberà JA, Bärtsch P, Bhattacharya J, Bhattacharya S, Bonsignore MR, Dewachter L, Dinh-Xuan AT, Dorfmüller P, et al. Pulmonary vascular endothelium: the orchestra conductor in respiratory diseases. *Eur Respir J*. 2018;51:1700745. doi: 10.1183/13993003.00745-2017
4. Vrints CJM, Krychtiuk KA, Van Craenenbroeck EM, Segers VF, Price S, Heidbuchel H. Endothelialitis plays a central role in the pathophysiology of severe COVID-19 and its cardiovascular complications. *Acta Cardiol*. 2021;76:109–124. doi: 10.1080/00015385.2020.1846921
5. Hoth M, Penner R. Depletion of intracellular calcium stores activates a calcium current in mast cells. *Nature*. 1992;355:353–356. doi: 10.1038/355353a0
6. Lewis RS. Store-operated calcium channels: from function to structure and back again. *Cold Spring Harb Perspect Biol*. 2020;12:a035055. doi: 10.1101/cshperspect.a035055
7. Lunz V, Romanin C, Frischauf I. STIM1 activation of Orai1. *Cell Calcium*. 2019;77:29–38. doi: 10.1016/j.ceca.2018.11.009
8. Prakriya M, Lewis RS. Store-operated calcium channels. *Physiol Rev*. 2015;95:1383–1436. doi: 10.1152/physrev.00020.2014
9. Putney JW Jr. A model for receptor-regulated calcium entry. *Cell Calcium*. 1986;7:1–12. doi: 10.1016/0143-4160(86)90026-6
10. Trebak M, Kinet JP. Calcium signalling in T cells. *Nat Rev Immunol*. 2019;19:154–169. doi: 10.1038/s41577-018-0110-7
11. Trebak M, Putney JW. ORAI calcium channels. *Physiology (Bethesda)*. 2017;32:332–342. doi: 10.1152/physiol.00011.2017
12. Abdullaev IF, Bisaillon JM, Potier M, Gonzalez JC, Motiani RK, Trebak M. Stim1 and Orai1 mediate CRAC currents and store-operated calcium entry important for endothelial cell proliferation. *Circ Res*. 2008;103:1289–1299. doi: 10.1161/01.RES.0000338496.95579.56
13. Lewis RS, Cahalan MD. Mitogen-induced oscillations of cytosolic Ca2+ and transmembrane Ca2+ current in human leukemic T cells. *Cell Regul*. 1989;1:99–112. doi: 10.1091/mbc.1.1.99
14. Berridge MJ. The inositol trisphosphate/calcium signaling pathway in health and disease. *Physiol Rev*. 2016;96:1261–1296. doi: 10.1152/physrev.00006.2016
15. Liou J, Kim ML, Heo WD, Jones JT, Myers JW, Ferrell JE Jr, Meyer T. STIM is a Ca2+ sensor essential for Ca2+-store-depletion-triggered Ca2+ influx. *Curr Biol*. 2005;15:1235–1241. doi: 10.1016/j.cub.2005.05.055
16. Roos J, DiGregorio PJ, Yeromin AV, Ohlsen K, Lioudyno M, Zhang S, Safrina O, Kozak JA, Wagner SL, Cahalan MD, et al. STIM1, an essential and conserved component of store-operated Ca2+ channel function. *J Cell Biol*. 2005;169:435–445. doi: 10.1083/jcb.200502019
17. Feske S, Gwack Y, Prakriya M, Srikanth S, Puppel SH, Tanasa B, Hogan PG, Lewis RS, Daly M, Rao A. A mutation in Orai1 causes immune deficiency by abrogating CRAC channel function. *Nature*. 2006;441:179–185. doi: 10.1038/nature04702
18. Vig M, Peinelt C, Beck A, Koomoa DL, Rabah D, Koblan-Huberson M, Kraft S, Turner H, Fleig A, Penner R, et al. CRACM1 is a plasma membrane protein essential for store-operated Ca2+ entry. *Science*. 2006;312:1220–1223. doi: 10.1126/science.1127883
19. Zhang SL, Yeromin AV, Zhang XH, Yu Y, Safrina O, Penna A, Roos J, Stauderman KA, Cahalan MD. Genome-wide RNAi screen of Ca(2+) influx identifies genes that regulate Ca(2+) release-activated Ca(2+) channel activity. *Proc Natl Acad Sci USA*. 2006;103:9357–9362. doi: 10.1073/pnas.0603161103
20. Emrich SM, Yoast RE, Trebak M. Physiological functions of CRAC channels. *Annu Rev Physiol*. 2022;84:355–379. doi: 10.1146/annurev-physiol-052521-013426
21. Yoast RE, Emrich SM, Trebak M. The anatomy of native CRAC channel(s). *Curr Opin Physiol*. 2020;17:89–95. doi: 10.1016/j.cophys.2020.07.012
22. Gwack Y, Feske S, Srikanth S, Hogan PG, Rao A. Signalling to transcription: store-operated Ca2+ entry and NFAT activation in lymphocytes. *Cell Calcium*. 2007;42:145–156. doi: 10.1016/j.ceca.2007.03.007
23. Benson JC, Trebak M. Too much of a good thing: the case of SOCE in cellular apoptosis. *Cell Calcium*. 2023;111:102716. doi: 10.1016/j.ceca.2023.102716
24. Curcic S, Schober R, Schindl R, Groschner K. TRPC-mediated Ca2+ signaling and control of cellular functions. *Semin Cell Dev Biol*. 2019;94:28–39. doi: 10.1016/j.semcdb.2019.02.001
25. Feske S. CRAC channelopathies. *Pflugers Arch*. 2010;460:417–435. doi: 10.1007/s00424-009-0777-5
26. Rinne A, Banach K, Blatter LA. Regulation of nuclear factor of activated T cells (NFAT) in vascular endothelial cells. *J Mol Cell Cardiol*. 2009;47:400–410. doi: 10.1016/j.yjmcc.2009.06.010
27. Blatter LA. Tissue specificity: SOCE: implications for Ca(2+) handling in endothelial cells. *Adv Exp Med Biol*. 2017;993:343–361. doi: 10.1007/978-3-319-57732-6_18
28. Dolmetsch RE, Xu K, Lewis RS. Calcium oscillations increase the efficiency and specificity of gene expression. *Nature*. 1998;392:933–936. doi: 10.1038/31960
29. Zhou MH, Zheng H, Si H, Jin Y, Peng JM, He L, Zhou Y, Muñoz-Garay C, Zawieja DC, Kuo L, et al. Stromal interaction molecule 1 (STIM1) and Orai1 mediate histamine-evoked calcium entry and nuclear factor of activated T-cells (NFAT) signaling in human umbilical vein endothelial cells. *J Biol Chem*. 2014;289:29446–29456. doi: 10.1074/jbc.M114.578492
30. Garcia-Vaz E, McNeilly AD, Berglund LM, Ahmad A, Gallagher JR, Dutius Andersson AM, McCrimmon RJ, Zetterqvist AV, Gomez MF, Khan F. Inhibition of NFAT signaling restores microvascular endothelial function in diabetic mice. *Diabetes*. 2020;69:424–435. doi: 10.2337/db18-0870
31. Giblin MJ, Smith TE, Winkler G, Pendergrass HA, Kim MJ, Capozzi ME, Yang R, McCollum GW, Penn JS. Nuclear factor of activated T-cells (NFAT) regulation of IL-1β-induced retinal vascular inflammation. *Biochim Biophys Acta Mol Basis Dis*. 2021;1867:166238. doi: 10.1016/j.bbadis.2021.166238
32. Wang Y, Hu J, Liu J, Geng Z, Tao Y, Zheng F, Wang Y, Fu S, Wang W, Xie C, et al. The role of Ca2+/NFAT in dysfunction and inflammation of human coronary endothelial cells induced by sera from patients with Kawasaki disease. *Sci Rep*. 2020;10:4706. doi: 10.1038/s41598-020-61667-y
33. Silva JDPD, Ballejo G. Pharmacological characterization of the calcium influx pathways involved in nitric oxide production by endothelial cells. *Einstein (Sao Paulo)*. 2019;17:eAO4600. doi: 10.31744/einstein_journal/2019AO4600
34. Trebak M, Vazquez G, Bird GSJ, Putney JW. The TRPC3/6/7 subfamily of cation channels. *Cell Calcium*. 2003;33:451–461. doi: 10.1016/s0143-4160(03)00056-3

35. Vazquez G, Wedel BJ, Aziz O, Trebak M, Putney JW. The mammalian TRPC cation channels. *Biochim Biophys Acta*. 2004;1742:21–36. doi: 10.1016/j.bbamcr.2004.08.015
36. Blair NT, Kaczmarek JS, Clapham DE. Intracellular calcium strongly potentiates agonist-activated TRPC5 channels. *J Gen Physiol*. 2009;133:525–546. doi: 10.1085/jgp.200810153
37. Trebak M, Lemonnier L, DeHaven WI, Wedel BJ, Bird GS, Putney JW. Complex functions of phosphatidylinositol 4,5-bisphosphate in regulation of TRPC5 cation channels. *Pflugers Arch*. 2009;457:757–769. doi: 10.1007/s00424-008-0550-1
38. Trebak M, Lemonnier L, Smyth JT, Vazquez G, Putney JW Jr. Phospholipase C-coupled receptors and activation of TRPC channels. In: *Handbook of Experimental Pharmacology*. 2007:593–614.
39. Freichel M, Suh SH, Pfeifer A, Schweig U, Trost C, Weißgerber P, Biel M, Philipp S, Freise D, Droogmans G, et al. Lack of an endothelial store-operated Ca2+ current impairs agonist-dependent vasorelaxation in TRP4-/- mice. *Nat Cell Biol*. 2001;3:121–127. doi: 10.1038/35055019
40. Qu YY, Wang LM, Zhong H, Liu YM, Tang N, Zhu LP, He F, Hu QH. TRPC1 stimulates calcium-sensing receptor-induced store-operated Ca2+ entry and nitric oxide production in endothelial cells. *Mol Med Rep*. 2017;16:4613–4619. doi: 10.3892/mmr.2017.7164
41. Clapham DE. Calcium Signaling. *Cell*. 2007;131:1047–1058. doi: 10.1016/j.cell.2007.11.028
42. Trebak M. STIM1/Orai1, ICRAC, and endothelial SOC. *Circ Res*. 2009;104:e56–e57. doi: 10.1161/CIRCRESAHA.109.196105
43. Chrzanowska-Wodnicka M. Rap1 in endothelial biology. *Curr Opin Hematol*. 2017;24:248–255. doi: 10.1097/MOH.0000000000000332
44. Boettner B, Van Aelst L. Control of cell adhesion dynamics by Rap1 signaling. *Curr Opin Cell Biol*. 2009;21:684–693. doi: 10.1016/j.ceb.2009.06.004
45. Wittchen ES, Aghajanian A, Burridge K. Isoform-specific differences between Rap1A and Rap1B GTPases in the formation of endothelial cell junctions. *Small GTPases*. 2011;2:65–76. doi: 10.4161/sgtp.2.2.15735
46. Lakshmikanthan S, Sobczak M, Li Calzi S, Shaw L, Grant MB, Chrzanowska-Wodnicka M. Rap1B promotes VEGF-induced endothelial permeability and is required for dynamic regulation of the endothelial barrier. *J Cell Sci*. 2018;131:jcs207605. doi: 10.1242/jcs.207605
47. Chrzanowska-Wodnicka M, White GC 2nd, Quilliam LA, Whitehead KJ. Small GTPase Rap1 is essential for mouse development and formation of functional vasculature. *PLoS One*. 2015;10:e0145689. doi: 10.1371/journal.pone.0145689
48. Birukova AA, Zagranichnaya T, Fu P, Alekseeva E, Chen W, Jacobson JR, Birukov KG. Prostaglandins PGE(2) and PGI(2) promote endothelial barrier enhancement via PKA- and Epac1/Rap1-dependent Rac activation. *Exp Cell Res*. 2007;313:2504–2520. doi: 10.1016/j.yexcr.2007.03.036
49. Altschuler D, Lapetina EG. Mutational analysis of the cAMP-dependent protein kinase-mediated phosphorylation site of Rap1b. *J Biol Chem*. 1993;268:7527–7531. doi: 10.1016/S0021-9258(18)53207-5
50. Lakshmikanthan S, Zieba BJ, Ge ZD, Momotani K, Zheng X, Lund H, Artamonov MV, Maas JE, Szabo A, Zhang DX, et al. Rap1b in smooth muscle and endothelium is required for maintenance of vascular tone and normal blood pressure. *Arterioscler Thromb Vasc Biol*. 2014;34:1486–1494. doi: 10.1161/ATVBAHA.114.303678
51. Lakshmikanthan S, Zheng X, Nishijima Y, Sobczak M, Szabo A, Vasquez-Vivar J, Zhang DX, Chrzanowska-Wodnicka M. Rap1 promotes endothelial mechanosensing complex formation, NO release and normal endothelial function. *EMBO Rep*. 2015;16:628–637. doi: 10.15252/embr.201439846
52. Kosuru R, Singh B, Lakshmikanthan S, Nishijima Y, Vasquez-Vivar J, Zhang DX, Chrzanowska M. Distinct signaling functions of Rap1 isoforms in NO release from endothelium. *Front Cell Dev Biol*. 2021;9:687598. doi: 10.3389/fcell.2021.687598
53. Shinde AV, Motiani RK, Zhang X, Abdullaev IF, Adam AP, González-Cobos JC, Zhang W, Matrougui K, Vincent PA, Trebak M. STIM1 controls endothelial barrier function independently of Orai1 and Ca2+ entry. *Sci Signal*. 2013;6:ra18. doi: 10.1126/scisignal.2003425
54. Stolwijk JA, Matrougui K, Renken CW, Trebak M. Impedance analysis of GPCR-mediated changes in endothelial barrier function: overview and fundamental considerations for stable and reproducible measurements. *Pflugers Arch*. 2015;467:2193–2218. doi: 10.1007/s00424-014-1674-0
55. Emrich SM, Yoast RE, Zhang X, Fike AJ, Wang YH, Bricker KN, Tao AY, Xin P, Walter V, Johnson MT, et al. Orai3 and Orai1 mediate CRAC channel function and metabolic reprogramming in B cells. *eLife*. 2023;12:e84708. doi: 10.7554/eLife.84708
56. Yoast RE, Emrich SM, Zhang X, Xin P, Johnson MT, Fike AJ, Walter V, Hempel N, Yule DI, Sneyd J, et al. The native ORAI channel trio underlies the diversity of Ca2+ signaling events. *Nat Commun*. 2020;11:2444. doi: 10.1038/s41467-020-16232-6
57. Livak KJ, Schmittgen TD. Analysis of relative gene expression data using real-time quantitative PCR and the 2(-Delta Delta C(T)) method. *Methods*. 2001;25:402–408. doi: 10.1006/meth.2001.1262
58. Singh B, Kosuru R, Lakshmikanthan S, Sorci-Thomas MG, Zhang DX, Sparapani R, Vasquez-Vivar J, Chrzanowska M. Endothelial Rap1 (Ras-association proximate 1) restricts inflammatory signaling to protect from the progression of atherosclerosis. *Arterioscler Thromb Vasc Biol*. 2021;41:638–650. doi: 10.1161/ATVBAHA.120.315401
59. Ferraresso F, Strilchuk AW, Juang LJ, Poole LG, Luyendyk JP, Kastrup CJ. Comparison of DLin-MC3-DMA and ALC-0315 for siRNA delivery to hepatocytes and hepatic stellate cells. *Mol Pharm*. 2022;19:2175–2182. doi: 10.1021/acs.molpharmaceut.2c00033
60. Urits I, Swanson D, Swett MC, Patel A, Berardino K, Amgalan A, Berger AA, Kassem H, Kaye AD, Viswanath O. A review of patisiran (ONPATTRO®) for the treatment of polyneuropathy in people with hereditary transthyretin amyloidosis. *Neurol Ther*. 2020;9:301–315. doi: 10.1007/s40120-020-00208-1
61. Parker JC, Townsley MI. Evaluation of lung injury in rats and mice. *Am J Physiol Lung Cell Mol Physiol*. 2004;286:L231–L246. doi: 10.1152/ajplung.00049.2003
62. Wang XX, Sha XL, Li YL, Li CL, Chen SH, Wang JJ, Xia Z. Lung injury induced by short-term mechanical ventilation with hyperoxia and its mitigation by deferoxamine in rats. *BMC Anesthesiol*. 2020;20:188. doi: 10.1186/s12871-020-01089-5
63. Sobczak M, Dargatz J, Chrzanowska-Wodnicka M. Isolation and culture of pulmonary endothelial cells from neonatal mice. *J Vis Exp*. 2010;46:2316. doi: 10.3791/2316
64. Takemura H, Hughes AR, Thastrup O, Putney JW Jr. Activation of calcium entry by the tumor promoter thapsigargin in parotid acinar cells. Evidence that an intracellular calcium pool and not an inositol phosphate regulates calcium fluxes at the plasma membrane. *J Biol Chem*. 1989;264:12266–12271.
65. Khan I, Sandhu V, Misquitta CM, Grover AK. SERCA pump isoform expression in endothelium of veins and arteries: every endothelium is not the same. *Mol Cell Biochem*. 2000;203:11–15. doi: 10.1023/a:1007093516593
66. Mountian I, Manolopoulos VG, De Smedt H, Parys JB, Missiaen L, Wuytack F. Expression patterns of sarco/endoplasmic reticulum Ca(2+)-ATPase and inositol 1,4,5-trisphosphate receptor isoforms in vascular endothelial cells. *Cell Calcium*. 1999;25:371–380. doi: 10.1054/ceca.1999.0034
67. Hadri L, Bobe R, Kawase Y, Ladage D, Ishikawa K, Atassi F, Lebeche D, Kranias EG, Leopold JA, Lompré AM, et al. SERCA2a gene transfer enhances eNOS expression and activity in endothelial cells. *Mol Ther*. 2010;18:1284–1292. doi: 10.1038/mt.2010.77
68. Zhang X, Xin P, Yoast RE, Emrich SM, Johnson MT, Pathak T, Benson JC, Azimi I, Gill DL, Monteith GR, et al. Distinct pharmacological profiles of ORAI1, ORAI2, and ORAI3 channels. *Cell Calcium*. 2020;91:102281. doi: 10.1016/j.ceca.2020.102281
69. Potier M, Gonzalez JC, Motiani RK, Abdullaev IF, Bisaillon JM, Singer HA, Trebak M. Evidence for STIM1- and Orai1-dependent store-operated calcium influx through ICRAC in vascular smooth muscle cells: role in proliferation and migration. *FASEB J*. 2009;23:2425–2437. doi: 10.1096/fj.09-131128
70. Fukushima M, Tomita T, Janoshazi A, Putney JW. Alternative translation initiation gives rise to two isoforms of Orai1 with distinct plasma membrane mobilities. *J Cell Sci*. 2012;125:4354–4361. doi: 10.1242/jcs.104919
71. Desai PN, Zhang X, Wu S, Janoshazi A, Bolimuntha S, Putney JW, Trebak M. Multiple types of calcium channels arising from alternative translation initiation of the Orai1 message. *Sci Signal*. 2015;8:ra74. doi: 10.1126/scisignal.aaa8323
72. Macian F. NFAT proteins: key regulators of T-cell development and function. *Nat Rev Immunol*. 2005;5:472–484. doi: 10.1038/nri1632
73. Mancini M, Toker A. NFAT proteins: emerging roles in cancer progression. *Nat Rev Cancer*. 2009;9:810–820. doi: 10.1038/nrc2735
74. El Chami H, Hassoun PM. Immune and inflammatory mechanisms in pulmonary arterial hypertension. *Prog Cardiovasc Dis*. 2012;55:218–228. doi: 10.1016/j.pcad.2012.07.006
75. Said SI, Hamidi SA, Gonzalez Bosc L. Asthma and pulmonary arterial hypertension: do they share a key mechanism of pathogenesis? *Eur Respir J*. 2010;35:730–734. doi: 10.1183/09031936.00097109
76. Johnson MT, Xin P, Benson JC, Pathak T, Walter V, Emrich SM, Yoast RE, Zhang X, Cao G, Panettieri RA Jr, et al. STIM1 is a core trigger of airway smooth muscle remodeling and hyperresponsiveness in asthma. *Proc Natl Acad Sci USA*. 2022;119:e2114557118. doi: 10.1073/pnas.2114557118
77. Moore TM, Norwood NR, Creighton JR, Babal P, Brough GH, Shasby DM, Stevens T. Receptor-dependent activation of store-operated calcium entry

increases endothelial cell permeability. *Am J Physiol Lung Cell Mol Physiol*. 2000;279:L691–L698. doi: 10.1152/ajplung.2000.279.4.L691

78. Zou M, Dong H, Meng X, Cai C, Li C, Cai S, Xue Y. Store-operated Ca2+ entry plays a role in HMGB1-induced vascular endothelial cell hyperpermeability. *PLoS One*. 2015;10:e0123432. doi: 10.1371/journal.pone.0123432
79. DebRoy A, Vogel SM, Soni D, Sundivakkam PC, Malik AB, Tiruppathi C. Cooperative signaling via transcription factors NF-κB and AP1/c-Fos mediates endothelial cell STIM1 expression and hyperpermeability in response to endotoxin. *J Biol Chem*. 2014;289:24188–24201. doi: 10.1074/jbc.M114.570051
80. Gudermann T, Steinritz D. STIMulating stress fibers in endothelial cells. *Sci Signal*. 2013;6:pe8. doi: 10.1126/scisignal.2004051
81. Cioffi DL, Stevens T. Regulation of endothelial cell barrier function by store-operated calcium entry. *Microcirculation*. 2006;13:709–723. doi: 10.1080/10739680600930354
82. Sukriti S, Tauseef M, Yazbeck P, Mehta D. Mechanisms regulating endothelial permeability. *Pulm Circ*. 2014;4:535–551. doi: 10.1086/677356
83. Stolwijk JA, Zhang X, Gueguinou M, Zhang W, Matrougui K, Renken C, Trebak M. Calcium signaling is dispensable for receptor regulation of endothelial barrier function. *J Biol Chem*. 2016;291:22894–22912. doi: 10.1074/jbc.M116.756114
84. Szulcek R, Bogaard HJ, van Nieuw Amerongen GP. Electric cell-substrate impedance sensing for the quantification of endothelial proliferation, barrier function, and motility. *J Vis Exp*. 2014;85:51300. doi: 10.3791/51300
85. Smith BJ, Bartolak-Suki E, Suki B, Roy GS, Hamlington KL, Charlebois CM, Bates JHT. Linking ventilator injury-induced leak across the blood-gas barrier to derangements in murine lung function. *Front Physiol*. 2017;8:466. doi: 10.3389/fphys.2017.00466
86. Rincon M, Irvin CG. Role of IL-6 in asthma and other inflammatory pulmonary diseases. *Int J Biol Sci*. 2012;8:1281–1290. doi: 10.7150/ijbs.4874
87. Rubini A. Interleukin-6 and lung inflammation: evidence for a causative role in inducing respiratory system resistance increments. *Inflamm Allergy Drug Targets*. 2013;12:315–321. doi: 10.2174/18715281113120500003
88. Jiang Y, Han S, Cheng W, Wang Z, Wu A. NFAT1-regulated IL6 signalling contributes to aggressive phenotypes of glioma. *Cell Commun Signal*. 2017;15:54. doi: 10.1186/s12964-017-0210-1
89. Nilsson LM, Sun ZW, Nilsson J, Nordström I, Chen YW, Molkentin JD, Wide-Swensson D, Hellstrand P, Lydrup ML, Gomez MF. Novel blocker of NFAT activation inhibits IL-6 production in human myometrial arteries and reduces vascular smooth muscle cell proliferation. *Am J Physiol Cell Physiol*. 2007;292:C1167–C1178. doi: 10.1152/ajpcell.00590.2005
90. Birukova AA, Tian X, Tian Y, Higginbotham K, Birukov KG. Rap-afadin axis in control of Rho signaling and endothelial barrier recovery. *Mol Biol Cell*. 2013;24:2678–2688. doi: 10.1091/mbc.E13-02-0098
91. Birukova AA, Meng F, Tian Y, Meliton A, Sarich N, Quilliam LA, Birukov KG. Prostacyclin post-treatment improves LPS-induced acute lung injury and endothelial barrier recovery via Rap1. *Biochim Biophys Acta*. 2015;1852:778–791. doi: 10.1016/j.bbadis.2014.12.016
92. Ke Y, Karki P, Zhang C, Li Y, Nguyen T, Birukov KG, Birukova AA. Mechanosensitive Rap1 activation promotes barrier function of lung vascular endothelium under cyclic stretch. *Mol Biol Cell*. 2019;30:959–974. doi: 10.1091/mbc.E18-07-0422
93. Yamamoto K, Takagi Y, Ando K, Fukuhara S. Rap1 small GTPase regulates vascular endothelial-cadherin-mediated endothelial cell-cell junctions and vascular permeability. *Biol Pharm Bull*. 2021;44:1371–1379. doi: 10.1248/bpb.b21-00504
94. Cioffi DL, Barry C, Stevens T. Store-operated calcium entry channels in pulmonary endothelium: the emerging story of TRPCS and Orai1. *Adv Exp Med Biol*. 2010;661:137–154. doi: 10.1007/978-1-60761-500-2_9
95. Wang G, Zhang J, Xu C, Han X, Gao Y, Chen H. Inhibition of SOCs attenuates acute lung injury induced by severe acute pancreatitis in rats and PMVECs injury induced by lipopolysaccharide. *Inflammation*. 2016;39:1049–1058. doi: 10.1007/s10753-016-0335-1
96. Li Y, Chen H, Shu R, Zhang X, Wang G, Yin Y. Hydrogen prevents lipopolysaccharide-induced pulmonary microvascular endothelial cell injury by inhibiting store-operated Ca2+ entry regulated by STIM1/Orai1. *Shock*. 2023;61:766–775. doi: 10.1097/shk.0000000000002279
97. Song X, Liu Y, Dong L, Wang Y. Stromal-interacting molecule 1 (Stim1)/Orai1 modulates endothelial permeability in ventilator-induced lung injury. *Med Sci Monit*. 2018;24:9413–9423. doi: 10.12659/MSM.911268
98. Cioffi DL, Lowe K, Alvarez DF, Barry C, Stevens T. TRPing on the lung endothelium: calcium channels that regulate barrier function. *Antioxid Redox Signal*. 2009;11:765–776. doi: 10.1089/ars.2008.2221
99. Gandhirajan RK, Meng S, Chandramoorthy HC, Mallilankaraman K, Mancarella S, Gao H, Razmpour R, Yang XF, Houser SR, Chen J, et al. Blockade of NOX2 and STIM1 signaling limits lipopolysaccharide-induced vascular inflammation. *J Clin Invest*. 2013;123:887–902. doi: 10.1172/JCI65647
100. Yang K, Liu S, Yan H, Lu W, Shan X, Chen H, Bao C, Feng H, Liao J, Liang S, et al. SARS-CoV-2 spike protein receptor-binding domain perturbates intracellular calcium homeostasis and impairs pulmonary vascular endothelial cells. *Signal Transduct Target Ther*. 2023;8:276. doi: 10.1038/s41392-023-01556-8
101. Sahu I, Pelzl L, Sukkar B, Fakhri H, Al-Maghout T, Cao H, Hauser S, Gutti R, Gawaz M, Lang F. NFAT5-sensitive Orai1 expression and store-operated Ca(2+) entry in megakaryocytes. *FASEB J*. 2017;31:3439–3448. doi: 10.1096/fj.201601211R
102. Bergmeier W, Weidinger C, Zee I, Feske S. Emerging roles of store-operated Ca^{2+} entry through STIM and ORAI proteins in immunity, hemostasis and cancer. *Channels (Austin)*. 2013;7:379–391. doi: 10.4161/chan.24302
103. Mahaut-Smith MP. The unique contribution of ion channels to platelet and megakaryocyte function. *J Thromb Haemost*. 2012;10:1722–1732. doi: 10.1111/j.1538-7836.2012.04837.x
104. Münzer P, Tolios A, Pelzl L, Schmid E, Schmidt EM, Walker B, Fröhlich H, Borst O, Gawaz M, Lang F. Thrombin-sensitive expression of the store operated Ca(2+) channel Orai1 in platelets. *Biochem Biophys Res Commun*. 2013;436:25–30. doi: 10.1016/j.bbrc.2013.05.031
105. Pelzl L, Tolios A, Schmidt EM, Alesutan I, Walker B, Münzer P, Borst O, Gawaz M, Lang F. Translational regulation of the serum- and glucocorticoid-inducible kinase-1 (SGK1) in platelets. *Biochem Biophys Res Commun*. 2012;425:1–5. doi: 10.1016/j.bbrc.2012.07.026
106. Bos JL. Linking Rap to cell adhesion. *Curr Opin Cell Biol*. 2005;17:123–128. doi: 10.1016/j.ceb.2005.02.009
107. Qiu C, Liu W, Shi F, Fen M, Ren L, Qi H. Silencing of β1 integrin regulates airway remodeling by regulating the transcription of SOCE-associated genes in asthmatic mice. *Mol Med Rep*. 2017;16:2645–2651. doi: 10.3892/mmr.2017.6863
108. Badaoui M, Mimsy-Julienne C, Saby C, Van Gulick L, Peretti M, Jeannesson P, Morjani H, Ouadid-Ahidouch H. Collagen type 1 promotes survival of human breast cancer cells by overexpressing Kv10.1 potassium and Orai1 calcium channels through DDR1-dependent pathway. *Oncotarget*. 2018;9:24653–24671. doi: 10.18632/oncotarget.19065
109. Lakshmikanthan S, Sobczak M, Chun C, Henschel A, Dargatz J, Ramchandran R, Chrzanowska-Wodnicka M. Rap1 promotes VEGFR2 activation and angiogenesis by a mechanism involving integrin $\alpha v\beta_3$. *Blood*. 2011;118:2015–2026. doi: 10.1182/blood-2011-04-349282
110. Carmona G, Göttig S, Orlandi A, Scheele J, Bäuerle T, Jugold M, Kiessling F, Henschler R, Zeiher AM, Dimmeler S, et al. Role of the small GTPase Rap1 for integrin activity regulation in endothelial cells and angiogenesis. *Blood*. 2009;113:488–497. doi: 10.1182/blood-2008-02-138438